62-4-5

ASD-TDR-62-314

STUDY OF THE MECHANISM OF FAILURE OF ROCKET MATERIALS AND MATERIALS RESEARCH

TECHNICAL DOCUMENTARY REPORT No. ASD-TDR-62-314

MAY 1962

DIRECTORATE OF MATERIALS AND PROCESSES
AERONAUTICAL SYSTEMS DIVISION
AIR FORCE SYSTEMS COMMAND
WRIGHT-PATTERSON AIR FORCE BASE, OHIO

Project No. 7350, Task No. 735001

(Prepared under Contract No. AF 33(616)-7048
by the Armour Research Foundation of Illinois Institute of Technology
Chicago 16, Illinois
Y. Baskin, D. C. Schell, and W. K. Sumida, authors)

NOTICES

When Government drawings, specifications, or other data are used for any purpose other than in connection with a definitely related Government procurement operation, the United States Government thereby incurs no responsibility nor any obligation whatsoever; and the fact that the Government may have formulated, furnished, or in any way supplied the said drawings, specifications, or other data, is not to be regarded by implication or otherwise as in any manner licensing the holder or any other person or corporation, or conveying any rights or permission to manufacture, use, or sell any patented invention that may in any way be related thereto.

Qualified requesters may obtain copies of this report from the Armed Services Technical Information Agency, (ASTIA), Arlington Hall Station, Arlington 12, Virginia.

This report has been released to the Office of Technical Services, U.S. Department of Commerce, Washington 25, D.C., for sale to the general public.

Copies of this report should not be returned to the Aeronautical Systems Division unless return is required by security considerations, contractual obligations, or notice on a specific document.

800 - July 1962 - 41-1774 & 1775

Aeronautical Systems Division, Dir/Materials and Processes, Metals and Cermaics Lab, Wright-Patterson AFB, Chio.
Rpt Nr ASD-TDR-62-314. STUDY OF THE MECHANISM OF FAILURE OF ROCKET MATERIALS AND MATERIALS RESEARCH. Final report, May 62, 108p. incl illus., tables, 13 refs.

Unclassified Report

Rocket failure mechanisms in conjunction with the development of nozzle materials for solid propellant motors is discussed. Testing graphite in an oxy-acetylene torch and the effects of purity, density, orientation, and microstructure on erosion-resistance were evaluated. Erosion decreased with greater

(over)

1. Nozzle materials
2. Graphite
3. Refractory metals
I. AFSC Project 7350, Task 735001
II. Contract AF 33(616)-7048
III. Armour Research Foundation of Ill. Inst. of Technology, Chicago, Ill.
IV. Y. Baskin, D. C. Schell, W. K. Sumida
V. Aval fr OTS
VI. In ASTIA collection

purity. New graphite materials were developed and evaluated including hot pressed compositions and impregnated bodies.

Suitability of ZrC as a nozzle material was evaluated. Incorporation of Ta and W fibers in ZrC results in considerable improvement in resistance to thermal spalling although not sufficient to prevent cracking. Thoria-base bodies reinforced with W fibers were studied.

Ten promising materials were fabricated into rocket nozzles and tested in static motor stands. Erosion performance is presented along with analysis of failure mechanisms.

Aeronautical Systems Division, Dir/Materials and Processes, Metals and Cermaics Lab, Wright-Patterson AFB, Chio.
Rpt Nr ASD-TDR-62-314. STUDY OF THE MECHANISM OF FAILURE OF ROCKET MATERIALS AND MATERIALS RESEARCH. Final report, May 62, 108p. incl illus., tables, 13 refs.

Unclassified Report

Rocket failure mechanisms in conjunction with the development of nozzle materials for solid propellant motors is discussed. Testing graphite in an oxy-acetylene torch and the effects of purity, density, orientation, and microstructure on erosion-resistance were evaluated. Erosion decreased with greater

(over)

1. Nozzle materials
2. Graphite
3. Refractory metals
I. AFSC Project 7350, Task 735001
II. Contract AF 33(616)-7048
III. Armour Research Foundation of Ill. Inst. of Technology, Chicago, Ill.
IV. Y. Baskin, D. C. Schell, W. K. Sumida
V. Aval fr OTS
VI. In ASTIA collection

purity. New graphite materials were developed and evaluated including hot pressed compositions and impregnated bodies.

Suitability of ZrC as a nozzle material was evaluated. Incorporation of Ta and W fibers in ZrC results in considerable improvement in resistance to thermal spalling although not sufficient to prevent cracking. Thoria-base bodies reinforced with W fibers were studied.

Ten promising materials were fabricated into rocket nozzles and tested in static motor stands. Erosion performance is presented along with analysis of failure mechanisms.

Aeronautical Systems Division, Dir/Materials and Processes, Metals and Cermaics Lab, Wright-Patterson AFB, Ohio.
Rpt Nr ASD-TDR-62-314. STUDY OF THE MECHANISM OF FAILURE OF ROCKET MATERIALS AND MATERIALS RESEARCH. Final report, May 62, 108p. incl illus., tables, 13 refs.

Unclassified Report

Rocket failure mechanisms in conjunction with the development of nozzle materials for solid propellant motors is discussed. Testing graphite in an oxy-acetylene torch and the effects of purity, density, orientation, and microstructure on erosion-resistance were evaluated. Erosion decreased with greater purity. New graphite materials were developed and evaluated including hot pressed compositions and impregnated bodies.

Suitability of ZrC as a nozzle material was evaluated. Incorporation of Ta and W fibers in ZrC results in considerable improvement in resistance to thermal spalling although not sufficient to prevent cracking. Thoria-base bodies reinforced with W fibers were studied.

Ten promising materials were fabricated into rocket nozzles and tested in static motor stands. Erosion performance is presented along with analysis of failure mechanisms.

(over)

1. Nozzle materials
2. Graphite
3. Refractory metals
I. AFSC Project 7350, Task 735001
II. Contract AF 33(616)-7048
III. Armour Research Foundation of Ill. Inst. of Technology, Chicago, Ill.
IV. Y. Baskin, D. C. Schell, W. K. Sumida
V. Aval fr OTS
VI. In ASTIA collection

Aeronautical Systems Division, Dir/Materials and Processes, Metals and Cermaics Lab, Wright-Patterson AFB, Ohio.
Rpt Nr ASD-TDR-62-314. STUDY OF THE MECHANISM OF FAILURE OF ROCKET MATERIALS AND MATERIALS RESEARCH. Final report, May 62, 108p. incl illus., tables, 13 refs.

Unclassified Report

Rocket failure mechanisms in conjunction with the development of nozzle materials for solid propellant motors is discussed. Testing graphite in an oxy-acetylene torch and the effects of purity, density, orientation, and microstructure on erosion-resistance were evaluated. Erosion decreased with greater purity. New graphite materials were developed and evaluated including hot pressed compositions and impregnated bodies.

Suitability of ZrC as a nozzle material was evaluated. Incorporation of Ta and W fibers in ZrC results in considerable improvement in resistance to thermal spalling although not sufficient to prevent cracking. Thoria-base bodies reinforced with W fibers were studied.

Ten promising materials were fabricated into rocket nozzles and tested in static motor stands. Erosion performance is presented along with analysis of failure mechanisms.

(over)

1. Nozzle materials
2. Graphite
3. Refractory metals
I. AFSC Project 7350, Task 735001
II. Contract AF 33(616)-7048
III. Armour Research Foundation of Ill. Inst. of Technology, Chicago, Ill.
IV. Y. Baskin, D. C. Schell, W. K. Sumida
V. Aval fr OTS
VI. In ASTIA collection

FOREWORD

This report was prepared by Armour Research Foundation of Illinois Institute of Technology under USAF Contract No. AF33(616)-7048. The contract was initiated under Project No. 7350, "Refractory Inorganic Non-Metallic Materials," Task No. 735001, "Refractory Inorganic Nonmetallic Materials: Non-Graphitic." The work was administered under the direction of the Directorate of Materials and Processes, Deputy Commander/Technology, Aeronautical Systems Division, Wright-Patterson Air Force Base, Ohio. Lt. T. E. Lippart was the project engineer.

This report covers work done from 15 March 1960 to 15 December 1961.

ABSTRACT

The objective of this contract was the study of rocket failure mechanisms in conjunction with the development of nozzle materials for solid propellant motors. Study of graphite comprised the major part of the program, with emphasis on erosion mechanisms. Commercial and experimental graphite grades were tested in an oxy-acetylene torch and the effects of graphite purity, density, orientation and microstructure on erosion-resistance were evaluated. The effect of graphite purity appeared to overshadow all other features in the dynamic tests; erosion decreased with greater purity. Similar trends were not observed in oxidation studies conducted at temperatures up to 1900°C in static air or flowing atmospheres. Graphite density had the greatest influence on resistance to ablation in the arc plasma experiments. New graphite materials were developed and evaluated on the program, including hot pressed compositions and several impregnated bodies.

Subsidiary effort was directed toward evaluating the suitability of zirconium carbide as a nozzle material. The poor thermal shock-resistance of this material is a major obstacle to its use in nozzle applications. Incorporation of tantalum and tungsten fibers in ZrC results in considerable improvement in resistance to thermal spalling, although still not sufficient to prevent cracking. Minor effort was directed toward the study of thoria-base bodies reinforced with tungsten fibers.

Ten promising materials were fabricated into rocket nozzles and tested in static motor stands. Erosion performance is presented along with analysis of failure mechanisms.

PUBLICATION REVIEW

This report has been reviewed and is approved.

FOR THE COMMANDER

W. G. RAMKE
Chief, Ceramics and Graphite Branch
Metals and Ceramics Laboratory
Directorate of Materials and Processes

TABLE OF CONTENTS

LIST OF ILLUSTRATIONS

LIST OF ILLUSTRATIONS (cont'd.)

LIST OF ILLUSTRATIONS (cont'd.)

LIST OF TABLES

LIST OF TABLES (cont'd.)

I. INTRODUCTION

Lack of fundamental information on the behavior of nozzle materials in solid propellant rockets has been an important factor retarding material development in this vital area. The need for materials research was recognized by some of the defense agencies involved in solid rocket programs and attempts were made to fill the gap. This program on nozzle material failure mechanisms, first sponsored by the Air Force in 1957, represented such an effort and it has contributed significantly to a better understanding of the nozzle material problem.

Over eighty different refractory materials and material combinations, fired with different propellants, were carefully analyzed during the first two years to determine failure mechanisms or reasons for resistance to deterioration. Analytical techniques used for this purpose included chemical, metallographic, petrographic, spectroscopic and X-ray diffraction. Results of these investigations are summarized in two WADC technical reports and a supplement (Refs. 1, 2 and 3). Considerable information was accumulated concerning behavior of specific nozzle compositions fired with different solid propellants. This information indicated which materials might have reasonable expectation of successfully fulfilling requirements in certain rocket environments and suggested improvements in presently used nozzle materials.

This report describes studies conducted during the third year of the program, under a new contract. Research was concerned with the study of nozzle material failure mechanisms along with investigation and development of materials and materials systems for solid propellant rocket nozzles. Study of graphite comprised the major portion of the program, with emphasis on investigation of erosion mechanisms. Various commercial and experimental graphite grades were tested using an oxy-acetylene torch and plasma-jet. Since erosion in graphite is a very complicated phenomenon, supplementary studies were conducted along with the dynamic erosion experiments to separate the major mechanisms. The effect of graphite purity, density, orientation and microstructure on graphite erosion and oxidation were studied. In addition, several new graphite compositions were developed and evaluated on the program.

Subsidiary effort was directed toward investigation of refractory metal carbides for rocket nozzle applications. Zirconium

---

Manuscript released by the authors January 1962 for publication as an ASD Technical Report.

carbide is similar to other refractory metal carbides and was chosen as a representative material for the group. Dynamic erosion studies were performed on ZrC of different densities using the oxy-acetylene torch. Attempts were made to improve the poor thermal shock-resistance of ZrC by incorporating refractory metal fibers and powder.

A minor phase of the program was concerned with fabrication and study of several promising metal fiber-reinforced ceramic compositions. These included ThO_2 and ThO_2-ZrO_2 bodies reinforced with tungsten fibers.

Finally, ten new compositions were fabricated into nozzles for testing in solid propellant motors at Battelle Memorial Institute. After testing the fired samples were analyzed to determine failure mechanisms.

II. EXPERIMENTAL METHOD

A. Equipment

1. Oxy-Acetylene Torch

Several different test methods were considered for simulating erosion in solid propellant rocket nozzles. An oxy-acetylene torch was finally selected because of its simplicity and reliability; reference to the abundant literature on the subject confirmed this selection. The erosion test apparatus is shown in Figure 1 and employs an oxy-acetylene welding torch (Airco Style 800 coupled with No. 6 tip). The torch propagates a thin inner flame cone of about three-fourths inch in length with neutral and oxidizing fuel mixtures. Flow rates (in cfh) were measured by Fisher and Porter flowmeters with precision bore flowrator tubes (Nos. 2-F-1/4-16-5-13 for acetylene and 2-F-1/4-20-5-13 for oxygen). Both tubes were calibrated for use at 12 psi gage pressure and 70° F. The test specimen holder was mounted on a sliding rack to facilitate movement relative to the torch. Temperature was measured using a Leeds and Northrup optical pyrometer. Thermodynamic analysis and ballistic properties of the oxy-acetylene torch are given in the Appendix.

Preliminary dynamic erosion tests were conducted to determine a suitable sample configuration for studying graphite erosion. The three models considered were thick-walled cylinder, rod and disk. Dimensioned diagrams of the three configurations studied are shown in Figure 2.

Descriptive diagrams of the torch, in relation to the positions of test specimens, are shown in Figures 3 and 4. In all cases, after exposure, the specimen holder was pulled away from the flame, and the specimen water-quenched to prevent excessive oxidation on cooling.

A ceramic holder was designed to retain the heat around the thick-walled cylinder. Another similar cylinder was inserted behind the sample to prevent erosion of the end surface on the test piece. The front end of the specimen was mounted within a boron nitride insulator concentric with the torch tip. The thin flame cone propagated along the inner wall conducted heat to the surface by convection.

Essentially black body conditions existed at the sight holes, insuring fairly accurate temperature measurements. It must be pointed out that the sight holes were not incorporated as part of test specimens when the erosion tests were made. Attendant oxidation around the consumed sight holes would tend to increase the apparent erosion volume.

The tip of the inner flame cone impinged directly on the apex of the rod specimen. Since this method involves a higher temperature (not a black body), a graphite holder was used to dissipate heat and to prevent oxidation of the enclosed end. A thin graphite flame deflector was used to reduce erosion of the exposed holder surface.

Two methods of direct flame attack were employed on the disk-shaped specimen (Figure 4). The holder was designed to enclose all but the attacked surface of the specimen and to rapidly dissipate its heat by water-cooling coils. A thick-walled cylinder served to reduce the exposed area in back of the test piece. Sight hole temperature was read with the aid of a prism. In both cases, the flame tip was in contact at the center of the exposed face.

Preliminary experiments established that the thick-walled cylinder was the best configuration for this study. The major advantages of this shape were (a) the geometry closely simulates that of the rocket nozzle, (b) erosion volume can be readily measured, (c) accurate surface temperatures can be obtained, and (d) erosion and temperature profiles in radial and transverse directions can best be obtained with a concentric heat source.

2. Arc Plasma

An arc plasma unit, built by Foundation personnel (see Figure 5), was employed to study erosion under severe ablative conditions in an inert atmosphere. This apparatus affords the means of obtaining a very high temperature source generated, in principle, by the arcing of a high velocity stream of ionizable gas through an aperture of one of the electrodes. For this purpose, the aperture, or consumable electrode, consisted of a cylindrical graphite test specimen mounted within a graphite plate. The nonconsumable electrode was a 1/4 inch diameter tungsten rod.

Positive potential was applied to the consumable graphite electrode from the DC power supplied by a Miller Model 360 welding generator. A half-view section of the basic arc plasma unit is shown in Figure 6a. A dimensional diagram of the arc plasma test model is shown in Figure 6b. As the graphite material was consumed during the course of a run, the erosion volume was projected deeper into the bore, assuming the shape of the plasma jet; its final shape was determined by the characteristic material properties of the test specimen. In preliminary runs using argon gas, the condensation product of the ablated graphite was deposited down the length of the bore. The deposited graphite resembled a columnar arrangement of graphite needles radiating inwardly, thus constricting the bore diameter. The termination of the sight hole was located one-fourth inch from the arcing edge of the bore. Surface temperature was read prior to the consumption of the sight hole. Test specimens were capped with a consumable graphite jacket to prevent undue oxidation to its surfaces.

Nearly constant test conditions were employed in an effort to detect differences in ablation behavior between the various graphite grades tested. The stabilizing gas was fed into the arc plasma unit at a rate of 55 cubic feet/hour. Initiation of the arc was accomplished by moving the tungsten electrode near the arcing edge of the graphite test specimen. Following this, the rod was quickly pulled back to a stop maintaining a constant arc gap for all the samples.

3. Graphite Combustion Apparatus

The combustion apparatus was constructed for evaluating static oxidation of graphite, supplementing the erosion study. A one-inch I.D. ceramic tube was heated in a resistance furnace or by a high frequency induction using graphite as the susceptor. For static oxidation experiments, one end of the combustion tube remained open to the atmosphere and the other end was open through an 8 mm glass tubing (mounted in a rubber stopper) which permitted insertion of the thermocouple in the furnace. Accessories for controlled flow of gases over the sample included a pressure regulator, needle valve, and a pre-calibrated pyrex glass flowrator tube. The sample, placed in a heated alumina boat was introduced into the hot zone of the combustion tube, exposed for a definite time, and quenched in mercury. By this method, rapid gravimetric analysis could be made. Samples, whose transverse strength was being determined as a function of time and temperature, were given the same treatment.

B. Experimental Procedures

1. Measurements of Variables

The fuel ratio is given in terms of metered flow rate of oxygen to acetylene and could be varied to produce flames that were reducing (0.85-0.95), neutral (1.04-1.14), or oxidizing (1.15-1.70) (Ref. 4).

Volume measurements were made of the central hole of the thick-walled cylinders to determine volume change as a result of firing. Initial volume was obtained geometrically and fired volume was measured volumetrically using mercury as the liquid medium. Volume change is a good indicator of degree of erosion, and this method was used with all test specimens.

Weights of test specimens were taken both before and after firing to evaluate mass loss as a function of time and temperature. While weight loss results may have only qualitative significance in the dynamic erosion experiments, because of the occurrence of particle dislodgement, they are very important in the static oxidation tests and contribute to an understanding of the role of oxidation in graphite erosion.

Bulk density was calculated from geometric measurements. "Real" density determinations were made by the liquid displacement method using absolute methanol (Ref. 5). Methanol was vacuum-impregnated into the open pores of the graphite sample to obtain consistent displacement results. The relationship of bulk and liquid densities to the theoretical density of graphite indicated the relative amount of pores inaccessible to methanol in various graphite grades, or

$$\text{Per cent closed porosity} = \frac{d_{\text{theoretical}} - d_{\text{liquid}}}{d_{\text{theoretical}} - d_{\text{bulk}}} \times 100$$

2. Determination of Grain Orientation

Graphite orientation was determined by X-ray diffraction, using a technique developed on the program. This technique, while not as accurate as the one outlined by Bacon (Ref. 6), was sufficiently accurate for the present purpose and the results were more easily obtained.

In practice, flat samples were cut in both longitudinal and transverse directions in graphite stock. For extruded material, the longitudinal direction coincides with the grain, while in molded material the transverse direction lies along the graphite grain. Smeared graphite produced during sectioning and by handling and

whose presence would have given misleading orientation results, was removed prior to X-ray analysis by means of masking tape. This treatment, consisting of repeated application of the sticky side of the tape to the surface, was effective in removing almost all of the smeared material.

Samples were mounted in the X-ray diffractometer and a tracing was obtained containing the 004 and 110 reflections. The 004 reflections are produced by graphite platelets lying parallel to the surface, while the 110 reflections are produced by platelets oriented normal to the sectioned surface. By coincidence, the intrinsic intensities of the two reflections are about equal. Thus, the intensity ratio of the 004 to the 110 reflection is greater in the longitudinal direction than in the transverse direction for extruded material, with the reverse relationship holding true for molded material.

The anisotropy factor is obtained according to the following relationship:

$$\text{Anisotropy Factor} = \frac{\frac{I_{004\,\ell}}{I_{110\,\ell}}}{\frac{I_{004t}}{I_{110t}}}$$

where I represents the area under the diffraction peak, ℓ - longitudinal, and t - transverse (reference to the manner in which samples are sectioned). A value greater than one is characteristic of extruded material, with the number increasing with greater degree of orientation. A value under one is characteristic of molded material; the smaller the fraction is the more highly oriented is the material. A randomly oriented material would have a value of unity. There was good reproducibility of results on the same sample; however, some variation was noted among different samples of the same grade owing to small orientation differences within the test block. A specimen tabulation of orientation data for samples of ZT-3001 and TS-245 is shown in Table I.

The low mass absorption coefficient of graphite results in fairly significant penetration of X-rays. Therefore, the orientation data is obtained from a fair volume of material and is not limited to surface material, which might render the results of doubtful value. Calculations show that the "half-value thickness" for graphite, using CuK α radiation, is about 0.6 mm. At the 2θ angles for the 004 and 110 reflections this represents 0.3 mm and 0.4 mm penetration, respectively. The X-ray beam covers an area somewhat greater than two square centimeters.

III. RESULTS AND DISCUSSION

A. Graphite Study

1. Materials

Commercial and experimental graphites covering a wide range of properties were obtained from National Carbon Company. The material properties, along with those for hot pressed graphite developed at the Foundation are listed in Table II. The ZT grades are characterized by relatively high densities and low open porosities. The RT grades are coarse-grained with intermediate densities and permeabilities, whereas extruded grades TS and TS-245 have low densities and open pore structures. CCH grade was obtained by submitting samples of AUC to the vendor for purification at elevated temperatures.

A high degree of orientation, shown by their very low anisotropy values, is a concomitant of the densification and recrystallization of the ZT grades and hot pressed graphite. TSX and TS-245 are highly oriented grades primarily because of the use of highly acicular needle cokes as the aggregate. Comparison of the anisotropy factor of TSX with the reciprocal of that for ZT-4001 shows TSX to be slightly more anisotropic. Of course, the orientation characteristics of an extruded grade differ markedly from those of a molded grade. The former more closely resembles a bundle of fibers, whereas the molded type is like a stack of cards.

The ATJ material examined showed virtually no orientation, but this might be a local effect in the sample. Some variation in orientation probably exists across the block, although ATJ is not characterized by much preferred orientation.

Photomicrographs of some of the experimental grades are shown in Figures 7-12. The microstructural features of the various grades such as grain size, orientation and pore structure are clearly illustrated. The coarse-grained texture and open pore structure of grades TS-245 and TSX are incongruous in the light of the dynamic erosion results described later.

2. Material Development

a. Hot Pressed Graphite

Previous studies at the Foundation showed the usefulness of prepolymerized furfuryl alcohol as a graphite binder (Ref. 7). It was decided to fabricate samples of this composition for rocket nozzle evaluation. A mix consisting of petroleum coke and 15 w/o furfuryl alcohol resin was molded at 125°C and slowly heated to 1000°C in

accordance with conventional carbonizing procedures. The carbonized samples appeared sound, but severe laminations occurred upon graphitizing at 3000°C. This composition was next hot pressed in graphite molds to eliminate the flaws. Thermax insulation was used around the molds to achieve the high temperatures needed to graphitize the sample. The resulting sample was sound and had a density of 1.81 g/cc; its photomicrograph is shown in Figure 13. Higher density might have been achieved by using denser graphite punches and molds.

A number of changes were made in the green mix compositions and more dense mold and punch material was used to raise the density of the hot pressed graphite. Ten w/o of thermax was substituted for coke, since this substitution has previously been shown to result in improved density and strength (Ref. 7). High-density graphite was employed to make the molds and punches permitting the use of fabricating pressures and temperatures somewhat higher than those feasible with the less dense material. These combined changes enabled the achievement of much higher densities than those obtained previously; samples suitable for testing in the oxy-acetylene torch were made with densities above 2.0 g/cc. Figures 14 and 15 show photomicrographs of small samples of hot pressed graphite with a density of 2.05 g/cc. The material was highly oriented, with an anisotropy factor of 0.026. This makes it even more highly anisotropic than ZT-4001 (see Table II for comparisons with other graphite grades). In addition, the material has a very fine pore structure and is virtually gas-tight.

Small bars were cut from the hot pressed specimens and these were tested for flexural strength utilizing the three-point loading method. Tensile strength was determined using the "brittle ring technique" (Ref. 8), and strain gages were attached to cylinders and bars to obtain compressive and flexural elastic moduli, respectively. The property data, listed in Table III, show, among other features, the high degree of anisotropy of the hot pressed graphite. The strength values and elastic modulus with the grain compare favorably with other high-density graphites.

Attempts at hot pressing graphite bodies using a flour made by Continental Oil Company were unsuccessful. The samples were highly laminated and poorly bonded. X-ray photographs of the coke flour showed it to be highly graphitic, comparable to a natural graphite. Thus, it is unlikely that such a coke will bond well to the furfuryl resin binder. The tendency of the body to laminate is related to the platy nature of the coke as well as to its poor bonding characteristics.

Methods used to purify cokes must avoid changing their structure in any manner that would impair their bonding characteristics. While the Continental coke may be of higher purity than the Texas coke used in the other samples, its structural features were unsuitable.

b. Reinforced Graphite

Graphite fibers* were incorporated in the green mix to improve the strength properties of hot pressed graphite. Five weight per cent of fibers were substituted for half of the thermax content. It was thought that fiber incorporation would lead to improved overall strength, since individual fibers possess relatively high tensile strength. The fibers were very fluffy and appeared to be more abundant in the green mix than they actually were. Two additional parts of furfuryl resin were included to compensate for the high absorbency of the fibers. Hot pressing was carried out in the same manner as the other samples.

Densities of the order of 2.0 g/cc were obtained with these bodies. As seen in Figure 16, other than presence of fiber relic structures, the material has the same general appearance as other hot pressed specimens (although it is slightly more porous than the sample shown in Figure 14). Flexural strength data presented at the bottom of Table III show that fiber incorporation had little effect upon strength; the fibers appear to behave as ordinary graphite filler.

Attempts at incorporation of tungsten fibers in graphite did not result in successful bodies. Temperatures used in fabrication apparently exceeded the melting point of some of the tungsten-carbon eutectics, resulting in large amounts of molten material being forced out during hot pressing. X-ray analysis of the material showed it to be tungsten dicarbide. A photomicrograph of the specimen appears in Figure 17 and shows irregular patches of tungsten carbide trapped in pores. Moreover, the graphite matrix appears fairly porous. There seems to be little possibility for improving this composition owing to the poor refractoriness of compounds in the tungsten-carbon system, which does not permit utilization of sufficiently high fabricating temperatures to densify graphite.

The refractoriness of all the compounds and eutectics in the tantalum-carbon system precluded any squeezing out of material in the present pressing. It was felt that a skeletal structure of tantalum carbide would appreciably improve the strength and erosion-resistance of graphite. However, as seen in Figure 18, the high porosity of the body, particularly around the tantalum carbide fibers, more than offsets any increase in strength which the fibers might give.

---

* Cut from graphite cloth manufactured by National Carbon Company.

The central voids in the fibers are of interest and are thought to result from oxidation of the metallic fibers during early stages of firing. Oxidizing gases are released during pyrolysis of furfuryl alcohol which are known to oxidize metal carbides, and presumably would also attack tantalum. This type of structure occurs when thin steel fibers are oxidized. At higher temperatures, the oxide converts to the carbide by reacting with carbon in the immediate vicinity of fibers, thus weakening the body. Oxidation of tantalum fibers followed by carbidization at higher temperatures, with their harmful side effects, makes it appear doubtful that this composition can be improved.

3. Dynamic Erosion

a. Preliminary Tests

Experiments were initially conducted to establish the feasibility and reproducibility of the oxy-acetylene torch technique for studying dynamic erosion of graphite. Thick-walled cylinders with an internal bore of 0.375 inch were machined from a number of commercial graphite grades for these studies. Samples were tested in the torch for varied time intervals using three different oxygen-acetylene gas ratios.

Results are summarized in Table IV and include some of the physical properties of the materials. The data show some expected trends, such as increased erosion with longer time exposure and with the use of more oxidizing gas mixtures. Relatively little erosion takes place during the first three minutes of a run, since about one minute and a half elapse before internal surface temperatures reach 1900° C (see Figure 19). Graphite erosion does not reach significant proportions in these experiments until this surface temperature is attained. This is illustrated in Figure 20, which also shows the excellent correlation between surface temperature and degree of erosion. Dynamic erosion clearly appears to be a temperature-dependent process.

Since oxidation of graphite is probably the most important single component of the dynamic erosion process, it is not surprising that it increases with greater concentrations of oxygen in the flame. Little or no erosion occurred with the use of a reducing fuel ratio of 0.93. Close examination of samples tested with an acetylene-rich fuel mixture showed that some pyrolytic deposition of carbon occurred, resulting in decreased bore volume. The relatively low temperatures of the reducing flames is another factor which limited their erosiveness. Appreciable erosion takes place with the use of "neutral" gas ratios (O_2:C_2H_2 1.09) and significantly more occurred when the ratio was increased to 1.22.

The absence of correlation in these experiments between density and erosion-resistance was unexpected. ATJ graphite, which had

substantially higher densities than the extruded grades, exhibited erosion-resistance no better than most of the other grades and poorer resistance than two of them. This was even more surprising in view of the fact that ATJ had considerably more closed porosity than the extruded materials. These results are not in agreement with those obtained using cylinders with a 1/4 inch bore described later. No reasons for the discrepancy are apparent.

The effect of oxygen to acetylene ratio upon erosion is further seen in Table V. The small increase in liquid density with firing indicated that most of the attack upon this material was superficial and that little oxidation occurred in internal portions of the cylinder. Metallographic analysis performed on other samples similarly treated showed this assumption to be correct.

Much of the increase in erosion with the use of oxygen-rich gas mixtures is due to the higher oxygen concentration in the flames. However, part of the increase can be accounted for by the higher surface temperatures associated with the more oxidizing flames. Data on graphite surface temperatures for several fuel ratios and two bore diameters, shown in Table VI, reveal the significant influence of oxygen content on surface temperature. Increased burning of graphite with more oxidizing flames might account for the higher surface temperatures, although the flame temperature itself might conceivably rise with increased oxygen supply. Surface temperature was measured with an optical pyrometer and the values were obtained at the moment the sight holes were consumed, insuring that actual surface temperatures were read. The position of sight hole T_1 was located laterally 7/8 inch from the firing end of the specimen and sight hole T_2 was spaced 1/4 inch from T_1. The radial distance from the sight hole terminus to the internal wall of the bore was about 1/16 inch. Temperatures recorded in the table are mean values determined in several specimens of grades AGSR, CS and ATJ. As was expected, surface temperature in the smaller bore was higher than in the larger one. Within limits of experimental error, temperatures (practically black body) did not vary among the various grades or with the different directions of grain alignment.

Dynamic erosion tests performed on the extruded samples with a 3/8 inch diameter bore yielded somewhat variable erosion results. This variability was most probably a reflection of variations in microstructure from sample to sample, but may also have been due to non-reproducible experimental conditions. Improvements were made in the apparatus, and bore dimensions were reduced to 1/4 inch to improve reproducibility. The 1/4 inch bore diameter was more compatible with the flame dimensions. This was expected to reduce gas turbulence, which might vary from run to run. Moreover, increased erosion rates, which were expected with the smaller bore diameter, might further mitigate variability.

b. Testing of Commercial and Experimental Grades

Results of the dynamic erosion tests on specimens with the 0.250 inch diameter bore are listed in Table VII. A slight improvement in erosion reproducibility occurred with the reduction of specimen bore diameter. However, variability was probably mostly due to variations in microstructure from one specimen to another within the same grade. Grade CS-112 exemplifies this. It showed the greatest variability in the earlier tests (see Table IV) and also exhibited the greatest variability in these tests. Degree of erosion is much higher with the smaller bore diameter and this is attributed to the fact that higher surface temperatures occur with the 1/4 inch bore diameter than with the 3/8 inch one.

The CCH grade showed an appreciable reduction in erosion compared with the precursor AUC-1 material. This was due either to the purification effects or to the effects of heat treatment at elevated temperatures, which is a necessary condition for purification. ATJ graphite exhibited about the best erosion-resistance among the commercial grades. This would appear to be a reflection of the higher density of this material as compared to the other commercial graphites. However, the RT and ZT grades, which are considerably denser than ATJ, performed little or no better. Apparently, the density factor is not the overshadowing one in these tests, and this is further seen in the case of lower-density TS-245 and TSX. The latter grade was the outstanding performer under both neutral and oxidizing conditions, indicating that purity might be an important factor. The hot pressed graphite produced at the Foundation showed relatively poor erosion-resistance in spite of its high density.

Metallographic analysis was performed on the fired samples to obtain more information on the mechanisms of erosion. All of the grades showed the same type of surface attack. Photomicrographs of ATJ are shown in Figures 21 and 22 to illustrate the features observed in almost all of the graphites tested. The photomicrograph of unfired ATJ is shown for comparative purposes. Figure 22 reveals the superficiality of oxidativc attack. Surface grains show signs of severe erosion caused by oxidation and particle dislodgement, but within a short distance of the boundary layer the graphite exhibits a fresh unaltered appearance. Liquid density measurements indicate that oxidative attack is limited to material at the surface. Microscopically. there does not appear to be any difference between the appearance of material tested with neutral or oxidizing fuel ratios. The manner of attack also does not vary with orientation of the grain relative to the flame.

Dislodgement of particles becomes noticeable after the first three minutes of run and was most pronounced in the less erosion-resistant graphites. It showed up as a stream of nearly incan-

descent particles coming from the sample. It was postulated that these particles might represent the original coke aggregate with the less highly ordered binder phase being burned off. If this were the case, the particles should have been more graphitic than the bulk material. However, X-ray diffraction analysis of the particles failed to disclose any structural differences between them and the unfired precursor material. X-ray analysis of material taken from erosion surfaces also failed to show any structural differences or changes as a result of firing. These negative results either indicate that it is virtually impossible to distinguish the binder phase from the aggregate by X-ray diffraction or that the graphitized binder is as reactive as the graphitized aggregate.

c. Orientation Effects

Oxidation studies with graphite single crystals have shown that the basal surfaces (00ℓ) are comparatively inert, whereas the oxidation reaction occurs largely at other crystal faces which are composed primarily of edge atoms (Ref. 9). Therefore, since many of the experimental graphites tested were highly oriented, it appeared likely that sample orientation might affect firing performance. Reference to Table VIII shows that a bore machined longitudinally in a cylinder of ZT-3001 would show a much higher proportion of layer edges than one similarly machined in TSX, and would presumably be more reactive, all other factors being equal. On the other hand, a transverse bore in ZT-3001 would show a large amount of basal surfaces, although the high proportion found in a transverse section could not be attained.

Cylindrical test specimens were fabricated in both orientations to study the effect of orientation upon dynamic erosion. Specimens were subjected to the oxy-acetylene torch for seven-minute intervals using neutral and oxidizing flames. Results are presented in Table IX and indicate that, although there appears to be higher erosion for samples in which the bore intersects the grain, the effect of orientation is not overwhelming. Certainly the superior performance of TSX cannot be ascribed to this factor alone. In the case of molded materials, the trends of erosion with orientation observed with the neutral flame carry through with the oxidizing flame; if anything, the two extruded grades show the opposite trends.

A further study of orientation effects was conducted using an X-ray diffractometer on the same flat samples both before and after dynamic erosion. The torch was directed parallel to the specimen surface for sufficient time to produce significant erosion. Results of this study, listed in Table X, are not conclusive. For ZT-3001, there is an expected relative depletion of crystallites having layer edges normal to the surface cut across the grain. However, a small depletion of basal planes occurs in the surface cut parallel to the grain. Very small changes occur with TSX in both directions, but

in both cases there is a slight depletion of basal surfaces. In general, these results appear to confirm the relatively minor effect of orientation on erosion characteristics noted previously.

d. Effect of Chemical Purity

From the preceding section, it is clear that the excellent erosion behavior of TSX cannot be ascribed to orientation effects alone, since the erosion-resistance of TSX in the transverse direction (its poorest) is significantly better than that of any of the other grades in their best orientations. The factor responsible for erosion-resistance of TSX in these experiments must be a cogent one, as it overshadows the deleterious effects of low density and relatively open pore structure. Chemical purity was suspected as being the important factor, since TSX is a high-purity nuclear grade. Five of the experimental grades were submitted for quantitative spectroscopic analysis to test this hypothesis. Samples were machined to specific dimensions and mounted in a special device in which an argon envelope could be maintained around the sample. The inert atmosphere was needed to prevent reaction of the sample with atmospheric nitrogen to form cyanogen; formation of this gas is undesirable because some of its emission lines mask those of expected impurities.

Results of these analyses and average ones for three commercial grades are presented in Table XI, along with related erosion data. The data for TSX reveal a relatively low impurity content. The absence in TSX of detectable amounts of iron and vanadium, both of which are known to catalyze graphite oxidation (Ref. 9) might be an important factor contributing to its excellent erosion-resistance in these tests. The absence of detectable vanadium and the relatively low level of iron in TS-245 may also account for its moderately good resistance to erosion. The presence of small quantities of silicon in both TSX and TS-245 would not be expected to deleteriously affect their erosion-resistance. Silicon additions to graphite, which react to form SiC at elevated temperatures, are known to provide good oxidation protection for the basic material through the formation of impervious layers of silica. The substantially improved erosion behavior of CCH, as compared to AUC, is clearly ascribable to increased purity, since the two grades were identical in every other respect; samples of CCH were randomly selected from machined samples of AUC already on hand. It is difficult to conceive that physical properties of AUC could have been altered by the purification process. In the light of the apparent importance of chemical purity discussed earlier, the erosion behavior of the CCH grade was disappointing.

e. Doping Experiments

Dynamic erosion samples of TSX were doped with iron, calcium and titanium to further examine the relationship between chemical purity and erosion-resistance. Samples were vacuum-impregnated with chloride solutions of these elements. Samples were then dried and slowly moved through an inert atmosphere graphite furnace at 3000°C to drive off volatiles and to permit the impurities to react with the graphite. Samples of TSX, which had not been doped, were placed in the furnace for control purposes. Results of spectroscopic analysis and related erosion data are presented in Table XII. The existence of only small differences in impurity levels among the doped samples was unexpected in view of the differing impregnation treatments. It is possible that the original differences in impurity contents were reduced during the heat treatment at 3000°C. Impurities, vaporized from samples in the hot zone, could have been carried downstream by the inert gas flow and condensed on samples in cooler portions of the furnace. The control samples were the last ones treated and were not moved from the hot zone; thus the moving stream of inert gas did not allow condensation of impurities on them during cooling of the furnace.

Examination of the data in Table XII indicates that the presence of greater amounts of iron and titanium in the doped samples correlates with increased erosion. The greater erosion exhibited by the heat-treated material, as compared to untreated TSX, may be due to undetectable or unanalyzed impurities or may be within the limits of experimental error. Most of the doped samples show similar erosion behavior, reflecting similar impurity contents. The exception to this are the samples originally doped with all three elements. However, on the basis of spectroscopic analysis, there is no explanation for the severe erosion exhibited by these samples.

f. Impregnated Graphite

Efforts were made to improve erosion-resistance of the various graphite grades by impregnation with furfuryl alcohol monomer and a modified furfuryl impregnant, both relatively high coke-yielding impregnants. Successful impregnation would be expected to reduce oxidation by sealing off many of the pores and to improve resistance to particle dislodgement by increasing body strength. Samples were vacuum-impregnated with the resins, heated at 50°C to polymerize the resins, and then carbonized at 1000°C. This cycle was repeated a second time prior to baking at graphitizing temperatures (3000°C). Figure 23 shows a photomicrograph of TSX impregnated with furfuryl alcohol and subsequently graphitized; the light areas represent the impregnant (see Figure 12 for comparison with unfired TSX). Several samples, impregnated with furfuryl alcohol, were set aside after the second carbonization step to evaluate erosion performance of impregnated materials at this heat treatment stage.

Dynamic tests were conducted under two flame conditions employing a seven-minute firing period.

Table XIII lists density and porosity data and erosion performance for untreated and impregnated materials. In general, impregnation resulted in increased bulk densities with attendant decrease in liquid densities; hence, the pore volume inaccessible to methanol increased sharply. Impregnation, followed by baking at 3000°C, resulted in significant improvement in erosion-resistance for the commercial grades and TS-245, whereas no improvement occurred for the already resistant TSX grades. Erosion values (under neutral flame conditions) for impregnated samples which were only carbonized show behavior intermediate between that of untreated specimens and that of specimens which were impregnated and graphitized; under oxidizing conditions no improvement over untreated material was observed. Apparently the carbonized resin is chemically more reactive than the graphite. The modified furfuryl impregnant significantly improved the erosion performance of AUC graphite, even more than the furfuryl alcohol impregnation. This is attributed to the fact that the modified furfuryl impregnant has been found to exhibit higher residual carbon formation than that of furfuryl alcohol.

Impregnation of graphite by high coke-yielding resins, especially if followed by baking at graphitizing temperatures, shows promise for improving the erosion-resistance of graphite. This is clearly seen in the case of impregnated ATJ, which shows erosion-resistance comparable to that exhibited by untreated TSX.

4. Arc Plasma Experiments

Several experimental and commercial graphites were tested in an argon-stabilized arc-plasma apparatus for seven minutes to study the effects of pure ablation on these materials. Among the information desired was the temperature at which ablation becomes significant and the properties in graphite which are important with regard to ablation-resistance. Test results on the five grades are summarized in Table XIV. Surface temperature data given in the table were obtained with an optical pyrometer by sighting into small sight holes positioned about one-fourth of an inch above the center of the arc. The holes terminated close to the surface and temperatures were recorded just prior to the time they opened up. Since the holes were not located at the hottest part of the arc (due to construction of the apparatus), maximum temperatures attained by the ablating graphite were somewhat higher than those listed. The lower temperatures reported for ZT-3001 and RT-0008 samples is a result of the higher density and the preferred orientation of these two molded materials. All of the samples were machined with the central bore parallel to the extrusion or molding axis. Thus, for molded materials the radial thermal conductivity was

highest, whereas for the extruded grades, the longitudinal conductivity was highest. ATJ did not exhibit high radial thermal conductivity, possibly because of its low anisotropy.

As seen in Table XIV, ablation-resistance increases with greater graphite density. For one thing, a denser grade contains more material per specific volume to be vaporized. Secondly, increased thermal conductivity usually accompanies higher density and this results in greater dissipation of heat from the surface and this results in lower surface temperatures. In preliminary experiments, it was noted that little ablation occurred when temperatures observed in the sight holes did not exceed 2600°C. It was virtually impossible to determine whether the relatively high ablation-resistance exhibited by grades ZT-3001 and RT-0008 was due more to high density or to the relatively low temperatures occurring during the test.

It is highly unlikely that ablation occurred in the dynamic erosion tests involving the oxy-acetylene torch. Surface temperatures never exceeded 2000°C, even under the most severe conditions. These temperatures are insufficiently high to produce graphite ablation on the basis of observations made in the arc-plasma experiments.

5. Oxidation Studies

Since erosion of graphite is a very complicated phenomenon, parallel experiments were conducted to separate the major mechanisms. Oxidation studies comprised the main part of this effort because oxidation is the most important component of graphite erosion. Experiments were conducted both under static air conditions and under flowing oxidizing atmospheres. Static oxidation experiments were performed in a small tube furnace of limited air capacity and in a much larger globar furnace. The small tube furnace was also employed for the flowing atmosphere experiments.

a. Static Oxidation

Studies were conducted on commercial and experimental graphite grades using apparatus and techniques previously described; samples consisted of 3/8 inch cubes of the various materials. Results of experiments conducted in the small tube furnace are summarized in Table XV. Work on AUC graphite was not completed owing to the extreme friability of the oxidized samples. Although the commercial grades generally exhibited higher oxidation rates than the experimental graphites at 1000°C, the gap was narrower at 1250°C, and virtually non-existent at 1500°C. In contrast to the widely dissimilar behavior shown by these materials in dynamic erosion tests, the grades merely showed small differences in oxidation behavior under static conditions. The outstanding performance displayed by TSX

in dynamic erosion experiments was not repeated here. At the termination of the experiments it became obvious that the supply of oxygen to the samples in the tube furnaces was very limited, and this tended to mitigate any differences in intrinsic oxidation behavior between the materials. Consequently, this test could not bring out differences in oxidation characteristics of the various graphites which could be correlated with the dynamic erosion experiments. Nevertheless, liquid density measurements of the samples yielded interesting results. Despite differences in physical properties, almost all the materials show highest liquid densities when oxidized at 1000°C, with lower values resulting with oxidation at higher temperature levels. Some of the grades exhibited no measurable difference in liquid density between untreated material and samples fired at 1500°C, showing little opening up of internal pores when oxidation was conducted at the higher temperatures. Most of the graphites showed increasing oxidation rates at higher temperatures, but the increases were suppressed by the limited air supply available in the furnace.

Results of the static oxidation study performed in a larger system with more abundant air supply are presented in Table XVI. Samples were placed on a bed of alumina grains contained in a large, open silicon carbide box, oxidized for a thirty minute period at a desired temperature, and quenched in water. Only two temperature levels were employed in this test, 1000° and 1500°C. The specific oxidation rates obtained in this environment were much higher than those obtained in the smaller combustion tube. The rates show significantly increased values at the higher temperature levels for the four experimental grades tested. The more open system in the furnace results in more rapid diffusion of oxygen and combustion gases and this was expected to accentuate inherent differences in oxidation characteristics between the grades. These differences might be accentuated further in oxidation experiments involving flowing oxidizing gases. TSX appears to show slightly more oxidation resistance than the other grades tested, both at 1000°C and 1500°C.

Liquid density determinations on these samples again disclose that opening up of inaccessible pores through oxidation occurs to a much greater extent at 1000°C than at 1500°C, regardless of the higher oxidation rates at the higher temperatures. Particularly noteworthy is the close agreement between the liquid densities of similar materials at the same temperature treatment obtained from measurements involving different furnace configurations (see Table XV and XVI). The values obtained are reproducible and appear to be independent of oxidation rates. These results bear out the observations that oxidation of graphite becomes more superficial with rising temperatures. As a result of higher combustion activity occurring at the external pores and surfaces, the oxygen supply is limited to the internal pores of the material. In some

cases, equivalent liquid densities are observed for untreated material as for samples oxidized at 1500°C.

Photomicrographs were taken of samples oxidized in static air and a representative series are shown in Figure 24-26. In all cases, regions near the outer surface are shown. Interior regions were carefully examined under the binocular microscope, but were not photographed. The enlargement of pores as a result of oxidation of ATJ at 1000°C is seen in Figure 24. Attack was uniform across the sample with no indication of severe surface attack. Figure 25, a photomicrograph of ATJ subjected to static oxidation at 1250°C, shows severe surface oxidation with pore enlargement falling off with distance from the surface. Material fired at 1500°C showed even more pronounced surface attack (see Figure 26), with the interior regions appearing unaffected. These observations parallel the results of liquid density measurements described earlier, and show that oxidation of graphite becomes more superficial with increasing temperature.

b. Flowing Atmospheres

Concomitantly with the static oxidation tests, oxidation rates of various graphite grades were determined in flowing atmospheres. Flow rates of gases were measured by means of a calibrated pyrex flowrator tube containing a saturated solution of zinc chloride. Surface temperatures of the graphite cubes were read with an optical pyrometer; ambient temperatures were obtained by sighting on the alumina boat holding the sample. In flowing oxygen gas, the maximum temperature reached was 1770°C for a flow rate of 1.06 liters per minute; the corresponding ambient temperature was 1650°C. Higher flow rates of pure oxygen invariably produced a heating effect. In contrast, graphite surface temperatures, which were lower than the ambient ones, were observed in experiments employing dry air and carbon dioxide gas. Carbon dioxide gas was used for the purpose of more closely simulating the gas composition of the oxy-acetylene flame. However, no attempt was made to introduce water vapor to the flowing gases.

The data for this oxidation study are presented in Table XVII. Experimental results for the three gas compositions show an increase in the specific oxidation rate with increasing gas flow. No significant differences in oxidation behavior appeared among the various grades at these temperatures. TSX, doped with various impurities, exhibited oxidation rates in pure oxygen virtually the same as those of untreated TSX or the other grades. As noted earlier, liquid densities of the oxidized materials appear virtually unchanged from their respective unfired values. It was thought that differences in oxidation behavior between the graphites might result with the use of higher ambient temperatures. Therefore, attempts were made to carry out flowing atmosphere oxidation

experiments at 1900°C, thus approximating the temperatures obtained in dynamic erosion tests. An induction unit was specially adapted for this purpose. Testing was limited to two grades, TSX and ZT-4001, owing to experimental difficulties encountered at these temperatures. Pure oxygen was used and the individual runs were kept short to prevent excessive deterioration of refractories at these temperatures. Temperatures of the order of 1930°C were attained at the graphite surfaces and oxidation was rapid. Nevertheless, no difference in oxidation rates was noted between the two grades. Complete furnace breakdown prevented continuation of these tests.

One of the more interesting features of all of the oxidation tests is the very close similarity in oxidation behavior of the different grades. Neither purity nor density seemed to have affected oxidation rates in static or flowing atmospheres. The absence of correlation between the results of dynamic erosion tests and those of the oxidation studies is not understood. If the catalytic effect of impurities on oxidation was a significant factor in the dynamic tests, (as it appeared to be) it should have shown up in these tests also. It is possible that the impurity effect is significant only under certain conditions of high mass flow and in gas compositions occurring in a gas-oxygen torch. This assumption will have to remain untested, since it is impossible to simulate combustion conditions of an oxy-acetylene torch without resorting to the test used.

6. Strength Determinations

Shear strength measurements were conducted on untreated material and on samples oxidized at two different temperature levels. It was thought that such data would provide insight into the mechanisms of sample deterioration resulting from oxidation, which might bear directly on the matter of particle dislodgement during erosion.

Samples are cut from the stock in the manner illustrated below:

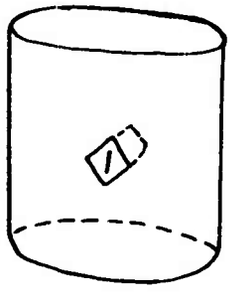

Each rectangular prism was sectioned and machined to a dimension of 3/8 x 3/8 x 3/16 inch. A diagonal reference line was marked on each specimen to indicate the direction of the long dimension of the stock. Orientation of the grain with respect to the reference line depended on whether the material was molded or extruded.

Shear strength measurements were conducted by breaking the specimen either parallel or perpendicular to the reference line by center beam loading over a span of one-eighth inch. The span on the apparatus was narrowed so that only the shear forces would be operating to produce failure; bending was practically negligible. Shear modulus was calculated by dividing one-half of the breaking load by the breaking cross section:

$$\text{Shear modulus} = \frac{P}{2\,bd}$$

where:

P = breaking load in pounds
b = breadth of the diagonal cross section in inches
d = depth or thickness in inches

Strength measurements were conducted on specimens treated in static air at 1000°C and 1500°C for thirty minutes. These samples were given the same static oxidation treatment as the test specimens described in Table XVI. The results of shear strength determinations as a function of grain orientation, and oxidation treatment are presented in Table XVIII, along with values determined for untreated materials. The high-density ZT grades possess greater original strength than the low-density TS grades; TSX is the weakest of the experimental grades tested. However, after oxidation at 1000°C, TSX exhibited the smallest decline in shear strength. This behavior of TSX is not repeated in material treated at 1500°C. Despite the fact that oxidation rates for all grades increased at 1500°C, the shear modulus values of the ZT grades are highest for samples oxidized at the more elevated temperatures. TS-245 exhibits about the same strength after oxidation at 1500°C as that after oxidation at 1000°C; TSX shows a drop in shear strength after oxidation at 1500°C, in comparison with treatment at the lower temperature.

These results are best understood by referring to the liquid density data on the same graphites presented in Table XVI. Greater internal deterioration occurs with oxidation at 1000°C than with oxidation at 1500°C, as is reflected in lower strengths for samples subjected to oxidation at 1000°C. Some of the ZT samples fired at 1500°C actually withstood greater loads before breaking than similar samples fired at 1000°C, despite the greater oxidation of the former.

There do not appear to be any clear cut relationships between shear strength and sample orientation. Shear strength across the grain would be expected to be higher than with the grain, but present results do not confirm this. Again, the results of this study do not show any correlation with the results of dynamic erosion, since all of the grades exhibit about the same deterioration in strength. TSX did not display greater resistance to deterioration than the other materials, although it did show the highest resistance to particle dislodgement in the dynamic erosion tests.

B. Carbide Study

Subsidiary effort in the program was directed toward obtaining more information concerning the suitability of refractory metal carbides for rocket nozzle applications. Although the carbide group contains some of the most refractory materials known, they have found virtually no application in solid propellant rockets because of certain inherent deficiencies. These are susceptibility to thermal shock and stress, brittleness, low oxidation-resistance, and poor fabricability. The objective of this phase of the program was to analyze and evaluate the performance of carbides in simulated nozzle tests. Investigations were limited to one carbide, ZrC; this material is similar in its properties to the other refractory metal carbides and is a representative material for the group.

Attempts were also made to improve upon the poor erosion-resistance and suceptibility to thermal shock of zirconium carbide through incorporation of refractory metal fibers or powder.

1. Materials and Material Development

Samples of zirconium carbide suitable for testing in the dynamic erosion apparatus were fabricated by hot pressing. Relatively high-purity powder (-325 mesh, 0.3% maximum free carbon), produced by Shieldalloy Corporation, was employed and samples were fabricated at temperatures ranging up to 2500°C under 2000 psi. Samples were made in two density ranges. One group had densities of about 75% of the theoretical value of 6.66 g/cc, whereas the other group had densities of about 90% of the theoretical value. Different hot pressing temperatures were employed to produce samples of the differing densities; thus the denser samples exhibited slightly coarser grain sizes. Specimens were also obtained commercially from Carborundum Company. These samples also had been fabricated by hot pressing and possessed densities averaging 98% of the theoretical value. Photomicrographs of the three types of ZrC are shown in Figures 27-29. The two higher density materials were etched to show grain size; etching had no effect on the porous ZrC. Both high-density materials showed similar grain size and pore size; they

only differed in the amount of porosity. The pores in both samples were mainly of the intragranular type, which is the hardest type to remove in sintering.

Zirconium carbide was reinforced with refractory metal fibers to improve its resistance to thermal spalling, as has been successfully done with thoria (Ref. 10). The degree of improvement of ZrC was not expected to be as great as that of thoria, since carburization of the fibers, an unavoidable occurrence, would render the fibers brittle, thus reducing their ability to inhibit crack propagation or to reinforce the carbide body. About 20% of short, thin (0.003 inch) fibers of tungsten and tantalum were mixed with zirconium carbide powder and hot pressed in graphite dies at temperatures up to 2500°C under 2000 psi. Photomicrograph of a sample containing tungsten fibers is shown in Figure 30. The fibers are surrounded by halos which are considerably denser than the zirconium carbide matrix. X-ray diffraction analysis revealed that the fibers become completely carbonized during hot pressing. Moreover, considerable diffusion of metal atoms also occurred, resulting in a fairly narrow range of WC-ZrC solid solution (ca. 45 at. % WC), with the rock-salt structure of zirconium carbide. Pure carbides of tungsten were not observed. X-ray analysis was only performed on bulk material and showed the existence of two phases. Consequently, it did not shed light on the composition of the material comprising the halo regions. Close examination of the photomicrograph suggests that the phase in the halo regions is zirconium carbide interspersed with small amounts of a lighter phase which is presumed to be the WC-ZrC solid solution. The light regions are not observed in the less dense ZrC matrix.

The formation of a relatively dense region of zirconium carbide surrounding the tungsten fibers suggested that tungsten may be used in moderate amounts to enhance sintering of this carbide. Additions of 20 w/o of fine tungsten powder were made to zirconium carbide and the samples were hot pressed in the usual manner. X-ray analysis revealed that complete reaction occurred between the two constituents to form a single WC-ZrC solid solution (with ca. 17 at. % WC). However, density measurements indicated that little improvement was achieved in the way of densification, since a maximum value of 86% of the theoretical figure for the composite was achieved. Densities of the order of 90-92% of the theoretical value have been obtained using essentially pure ZrC. Furthermore, the sample was also very brittle. Nature of the mechanism promoting densification in the halo regions is not understood, nor is the reason why similar densification should not occur in powdered compacts.

Photomicrograph of a sample of zirconium carbide reinforced with tantalum fibers is shown in Figure 31. Thin reaction zones

occur at the fiber-matrix boundaries, but dense regions in the matrix around the fibers are not observed. X-ray diffraction revealed that the tantalum had been completely transformed into the monocarbide (TaC), and that, in contrast to the situation with compacts containing tungsten fibers, negligible reaction occurred between the two carbides.

2. Dynamic Tests

Thick-walled cylinders of each ZrC type (1-inch O.D., 0.375-inch bore) were tested in the dynamic erosion apparatus using neutral and oxidizing flames. The results of these tests are summarized in Table XIX. All of the unreinforced samples cracked at the onset of the run, suggesting failure by thermal shock. The poor resistance of zirconium carbide to thermal shock and stress makes it highly susceptible to this type of failure and the tendency is accentuated in these tests, owing to the use of relatively thick-walled cylinders.

The fact that all of the unreinforced samples cracked in testing suggests that sample density had little effect upon thermal shock-resistance. This problem does not seem readily soluble for unreinforced thick-walled, cylindrical shapes. An alternative is to reduce wall thickness to the point where thermal gradients are sufficiently low so that the resulting thermal stress levels can be tolerated by zirconium carbide. Conventional thermal stress calculations for this material show that, in the temperature range 1000-1200°C, cracking will ensue if the thermal gradient across the 0.312-inch wall exceeds about 60°C. Measured thermal gradients in the tests ranged from 220-350°C, considerably higher than the tolerable value. A thinner walled cylinder would certainly have a better chance of withstanding thermal stresses, although it would be more difficult to fabricate such a configuration by usual means. However, it should be pointed out that these calculations relate to thermal stress, whereas the mode of cracking of the samples is probably by thermal shock. It would require more involved calculations to estimate the dimensions and configurations of zirconium carbide nozzles which would resist cracking from thermal shock. The accuracy of such calculations would be in doubt owing to the variability in properties of the material. Furthermore, thermal shock equations, in their present state, do not yield definitive results.

Despite the small amount of cracking of the reinforced ZrC samples, pronounced improvement in thermal spalling-resistance was obtained with the incorporation of metal fibers. Cracks that formed were small and the samples possessed adequate structural integrity. The fibers still had some ability to act as crack stoppers, although not to the same extent as that of uncarburized metal fibers.

Oxidation did not appear to be a major problem for the dense samples. A thin coating of zirconia (monoclinic) forms in the bore, much of it when the sample cools. Particle dislodgement is practically negligible and there is little enlargement of the bore. As might be expected, oxidation is serious for the low density, high porosity samples, and more oxidation takes place with use of more oxidizing flames.

C. Ceramic Oxides

Work on refractory oxides was mainly concerned with fabrication of nozzles from promising metal-reinforced compositions, including some materials research. Previous unreported tests revealed that stabilized zirconia nozzles reinforced with tungsten fibers exhibited poor performance in solid propellant rockets. Poor behavior was attributed to insufficient refractoriness of the stabilized ZrO_2 (melting point about 2300°C). There was an apparent need for more refractory oxides, such as ThO_2, alone or in combination with other ceramics.

Compacts composed of equal molecular proportions of thoria and monoclinic zirconia were hot pressed at 1500°C under 2000 psi. It was thought that a $ThO_2 \cdot ZrO_2$ composition would exhibit lower expansivity without significant sacrifice in refractoriness. Lower expansivity for the ceramic is desirable for reinforced compacts because it reduces the concentration and size of microcracks (Ref. 10). X-ray diffraction revealed that negligible reaction occurred between the two oxides at the temperature used in fabrication. The pattern for the high-purity monoclinic zirconia remained unchanged with firing. Surprisingly, the specimen retained structural integrity despite the fact that the zirconia underwent the destructive tetragonal to monoclinic transition. The occurrence of zirconia as a dispersed phase in a thoria matrix undoubtedly explains the fact of structural integrity.

Continuing the study of the ThO_2-ZrO_2 combination, samples consisting of 90 volume per cent of the oxides plus 10 volume per cent of tungsten fiber (0.005-inch) were fabricated. Using the dynamic method, Young's modulus of elasticity was calculated from the equation:

$$E = CWf^2$$

where E = Young's modulus, C = shape factor, W = weight in pounds, and f = fundamental frequency.

The moduli for two control samples were 12.74×10^6 and 13.16×10^6; for the two fiber containing samples they were 15.27×10^6 and 15.58×10^6. The samples were then placed in

a furnace and the dynamic modulus of elasticity was measured on both the heating and cooling cycle. These data are plotted in Figures 32 and 33. The $ThO_2 \cdot ZrO_2$ compacts showed a drop in modulus in the inversion range of zirconia (Figure 32). The moduli then show an increase to 1500°C, the maximum temperature reached during this run. On cooling, one sample followed somewhat the same pattern displayed on heating, with a sharp drop in modulus between 850°C and 800°C. The second sample displayed erratic behavior through the inversion range.

Of the two samples reinforced with fibers, one showed a general increase in modulus over the temperature range 500°C to 900°C and then appeared to level off at 1500°C. Modulus values followed much the same path on cooling.

The second reinforced specimen (see Figure 33) displayed an irregular but slowly increasing elastic modulus to roughly 1250°C. However, when heated to higher temperatures, the value dropped rapidly between 1650°C and 2000°C, the maximum temperature studied. On cooling, the modulus increased rapidly between 2000°C and 1400°C; it then dropped slowly, approaching the original value at room temperature. The last specimen, heated to 2000°C, showed evidence of deformation.

D. Rocket Nozzle Testing

1. Nozzle Fabrication

Rocket nozzles were fabricated from ten promising developed materials for testing in a solid propellant facility at Battelle Memorial Institute. Approximately twenty propellant grains have been made available at Battelle for this purpose and small nozzles of relatively simple design (1-1/2 inch O.D., 3/8 inch throat diameter) were machined in accordance with motor specifications. The materials and some of their properties are listed in Table XX. Two additional materials, ZT-4001 and TSX, were submitted for the purpose of determining whether or not any correlation exists between behavior in a solid propellant test and that in the oxy-acetylene test. All of the zirconium carbide samples and the two hot pressed graphites were fabricated at 2500°C under 2000 psi. Similar fabrication pressures were used for the thoria samples, but temperatures of the order of 1500°C were employed. For both the ZrC and ThO_2 nozzles, the center hole was drilled by ultrasonic method using a Raytheon Impact Grinder. The entrance cone was machined with diamond tools. Impregnation of the graphite samples was carried out in the manner described earlier. Finally, two nozzle compositions were coated with a thin layer of tungsten by Dr. Charles Barnes, Electronic Technology Laboratory, A.S.D.; coating was accomplished by a vapor

deposition process. Difficulties encountered in applying the coating limited the number of coated samples to one each of the two compositions. As noted in Table XX, a thoria nozzle and some of the zirconium carbide nozzles were cracked prior to firing as a result of fabrication difficulties. Lack of time did not permit the fabrication of additional nozzles.

2. Testing Procedures

Nozzles were statically tested in conventional rocket motors using solid propellants manufactured by Thiokol Chemical Corporation (PBAA-ammonium perchlorate-aluminum) and Hercules Powder Company (HDDQ-aluminized). All information pertaining to test equipment, propellant composition and characteristics, motor performance and other relevant particulars of the tests are described in detail in a WADD technical report (Ref. 11) and a quarterly report issued by Battelle Memorial Institute (Ref. 12). This information is not included in this report owing to classifications reasons.

Chamber pressure and thrust curves and photographs of the tested nozzles were supplied by the firing contractor. Original plans called for 10-second firings using 600 psi chamber pressure. These conditions were met in many tests, but nozzle deterioration, and occasionally alumina-aluminum deposit buildup resulted in departures from the desired parameters.

3. Test Results

Results of the solid propellant firings are summarized in Table XXI. Generally, greater erosion took place with the use of the Hercules propellant, despite the fact that chamber pressures occurring in these tests were invariably lower than the pressures in tests employing the Thiokol propellant. Higher chamber pressures usually results in increased nozzle erosion and deterioration.

The Hercules propellant appears to burn at higher flame temperatures and may also release more erosive exhaust products. Aluminum metal, as well as alumina, was observed in deposits of all of the nozzles tested with the Hercules propellant; only alumina was found in nozzles fired with the Thiokol propellant.

ZT-4001 and the two hot pressed graphites showed little or no erosion. In fact, they actually showed a decrease in throat area, possibly due to exhaust deposit buildup. However, the hot pressed graphite nozzles, particularly those containing graphite fibers, exhibited significant transverse cracking. Untreated TSX displayed moderate erosion, showing slight improvement in erosion-resistance with impregnation. The outstanding behavior in the oxy-

acetylene tests described previously was not repeated here; moreover, its order of merit with respect to ZT-4001 was reversed in the present tests. ATJ samples impregnated with furfuryl alcohol and the modified furfuryl impregnant showed fair resistance to erosion. However, since untreated ATJ was not tested at this time, it was not possible to assess the degree of improvement imparted by this impregnant. The zirconium carbide and thoria nozzles were severely eroded, the former also showing considerable cracking. It is evident that the improvement in thermal spalling-resistance of ZrC resulting from incorporation of tungsten or tantalum fibers is not sufficient to prevent the nozzles from cracking in these tests. In spite of some flaws, the tungsten coatings visibly improved the erosion-resistance of reinforced ZrC and ThO_2. However, some of the improvement may be more apparent than real since the latter tests involved lower chamber pressures than those in which uncoated samples were tested.

4. Analysis of Failure Mechanisms

Fired nozzles were carefully analyzed to determine failure mechanisms. Analytical techniques employed included metallographic, petrographic and X-ray diffraction. Detailed description of the analytical methods and procedures are outlined in two previous WADC technical reports (Refs. 1 and 3).

a. Hot Pressed Graphite

Virtually no erosion occurred with this material in the solid propellant tests, in contrast with behavior in the oxy-acetylene torch. The presence of relatively large amounts of vanadium in the graphite did not have deleterious effects on firing behavior in the solid propellant tests. The small amount of erosion that occurred was a result of superficial intergranular attack (see Figure 34).

Macroscopic cracking in the transverse direction was the most serious mechanism of failure of this material. The developed fracture patterns suggested thermal stress as the cause of cracking. The highly anisotropic nature of this graphite makes it particularly susceptible to transverse thermal cracking for two reasons. First, the hot pressed material has comparatively low transverse strength because of its preferred orientation to the nozzle axis (which was also the pressing axis). Second, stresses in the transverse direction are greatest owing to the high axial thermal expansion coefficient. Thus, transverse cracking should become more pronounced with the use of more highly anisotropic material. Such a trend has been observed with ZT nozzles, where cracking became more serious with higher density and anisotropy. (Ref. 13).

X-ray diffraction showed the presence of alpha-alumina in the exhaust deposits of both nozzles. Aluminum was additionally found in the nozzle tested with Hercules propellant.

b. Untreated TSX

TSX graphite did not crack on firing, but exhibited moderate erosion. The coarse microstructure and relatively low density of this material resulted in substantial intergranular attack, and presumably particle dislodgement (Figure 35). Density appears to be the most important feature affecting erosion-resistance of graphite in the solid propellant tests; graphite purity was of secondary or lesser importance. As before, alumina and aluminum constituted the exhaust products.

c. Zirconium Carbide with Tungsten Fibers

This material was severely cracked and eroded in the tests as a consequence of its poor resistance to thermal shock and stress. Erosion was primarily due to thermal spalling. It is considered unlikely that melting of the material occurred during the short firing interval and little oxidation was observed. Clearly, incorporation of fibers did not sufficiently improve the thermal shock-resistance of ZrC to enable it to withstand the conditions of the tests.

X-ray diffraction showed the fibers to be mainly composed of tungsten monocarbide, with little interaction between them and the ZrC matrix; considerable interaction was observed between fibers and matrix in earlier experiments (see Section B). Variation in sample size and fabrication parameters are presumed to be responsible for the differences in material interaction. Small amounts of zirconium oxide were observed in the X-ray photographs, indicating negligible oxidation; it is possible that even this oxidation occurred on cooling. Again, alpha-alumina and aluminum (in Hercules rockets) were observed, although rapid spalling did not provide much opportunity for deposit buildup.

d. Zirconium Carbide with Tantalum Fibers

Poor firing behavior of this composition is also a result of its susceptibility to thermal spalling. No melting was observed and oxidation was negligible. The extent of cracking can be seen in the dark photomicrograph shown in Figure 36. Again, the fibers did not improve the resistance to thermal spalling of ZrC sufficiently to enable it to withstand cracking in these tests.

X-ray diffraction showed the fibers to be tantalum monocarbide, as before. Small amounts of alpha-alumina and aluminum were also found. No zirconium oxide was detected, indicating little oxidation.

e. Thorium Oxide with Tungsten Fibers

This composition exhibited moderately severe erosion in the tests. However, the nozzles survived during firing without gross failure, which would have been impossible with unreinforced thoria. The erosion-resistance of this material was not satisfactory owing to the presence of numerous microcracks in the thoria matrix. The microcracks occur in unfired material as a result of stresses that develop on cooling from hot pressing temperatures due to differences in thermal expansion coefficients between thoria and tungsten (Ref. 10). The fibers serve to keep the body together and prevent formation of major cracks. However, the small fragments are not held together with sufficient strength to withstand the high-velocity gas stream. Figure 37 shows the irregular throat surface produced by dislodgement of the weakly-held particles; the fibrous skeletal network remains intact for some time after the particles have been ejected. These fibers become dislodged when the grains and fibers holding them no longer grip them adequately.

X-ray diffraction showed the fibers in fired nozzles still to be unreacted tungsten. Small amounts of tungsten oxides (WO_3, etc.) were detected and the exhaust deposits consisted of alumina and aluminum (Hercules).

f. Hot Pressed Graphite with Graphite Fibers

Although little erosion occurred with this nozzle composition, transverse cracking was very serious. The highly anisotropic nature of the matrix made it susceptible to this type of failure, as discussed earlier. Furthermore, the presence of fibers accentuated susceptibility to cracking since areas of high fiber concentrations represent zones of weakness. This is seen in Figure 38, where a cluster of fiber ends can be observed along a fractured surface. Fibers were also seen prominently associated with cracks in other areas of the nozzle. Exhaust deposit buildup of alumina and aluminum was moderately extensive.

g. ZT-4001

Virtually no erosion occurred with this material and the fired nozzles were uncracked. Figure 39 shows a smooth throat surface, exhibiting no intergranular attack. As mentioned earlier, graphite density is the most important property affecting erosion-resistance in the solid propellant tests (in contrast to the oxy-acetylene tests). Buildup of alumina and aluminum was relatively extensive, causing some constriction in the throat diameter.

h. TSX Impregnated with a Modified Furfuryl Impregnant

This composition exhibited moderate erosion and no cracking. Impregnation appears to have reduced the severity of intergranular attack on this material (see Figure 40 and compare with Figure 35). Small deposits of alumina and aluminum were detected.

i. ATJ Impregnated with a Modified Furfuryl Impregnant

This composition also showed little to moderate erosion with no cracking. As seen in Figure 41, there are signs of moderate intergranular attack at the throat surface. Impregnation of ATJ with the modified furfuryl compound is presumed to have been beneficial; however, this cannot be verified as untreated control nozzles were not tested. The usual exhaust products were detected by X-ray diffraction.

j. ATJ Impregnated with Furfuryl Alcohol

This composition also exhibited little erosion and no cracking in the tests. Photomicrograph of a fired nozzle is not included because of its similarity to Figure 41. It is also presumed that impregnation with furfuryl alcohol improved the erosion-resistance of ATJ.

k. Zirconium Carbide with Tungsten Fibers Coated with Tungsten

The tungsten coating did not reduce cracking in the matrix, although it did temporarily protect the bulk material from erosion. Nevertheless, rapid deterioration ensued in the exit portion of the throat after the coating was destroyed. Figure 42 illustrates the manner in which subsequent deterioration occurred in unprotected areas. It was hoped that the metallic coating, because of its relatively high thermal conductivity, would spread the heat uniformly and lessen thermal shock on the carbide. The presence of cracks in regions protected by the coating shows that thermal shock was still too great. Cracks which first developed were internally supported by the coating which also protected the matrix from direct contact with the exhaust gases. Eventually, the cracked substrate led to cracking of the coating followed by its destruction and the nozzle deteriorated rapidly by dislodgement of large pieces. In this nozzle coating cracks were originally present.

X-ray diffraction showed the tungsten coating to be chemically unaffected by firing. The original tungsten fibers had been transformed to tungsten monocarbide during fabrication and little interaction occurred between fibers and the ZrC matrix. No

zirconia or tungsten oxides were detected, again demonstrating the minor amount of oxidation that occurred in this rocket environment.

1. Thorium Oxide with Tungsten Fibers Coated with Tungsten

The tungsten coating probably protected this composition for a time. However, due to poor bonding with the substrate or because of coating flaws, it was destroyed in the throat region. Deterioration of the reinforced thoria then proceeded in the manner described previously for uncoated material (Figure 43). X-ray diffraction failed to uncover any crystalline compounds other than the original constituents or alumina from the propellant.

IV. CONCLUSIONS

1. High-density graphite bodies can be fabricated in several hours by direct hot pressing of the green mix. The material is strong, highly anisotropic, and can be made with densities ranging up to 2.05 g/cc. Incorporation of graphite fibers had little effect on compact strength, whereas incorporation of tantalum or tungsten fibers actually reduced body density and strength.

2. TSX showed the least erosion in the dynamic erosion tests under both neutral and oxidizing flame conditions. It outperformed experimental materials of the ZT series, which were considerably denser and possessed superior microstructure. The excellent erosion-resistance of TSX in the oxy-acetylene tests is attributed to its very low impurity content (as shown by spectroscopic analysis). The presence of small amounts of iron and vanadium in the other grades is believed responsible for catalyzing oxidation of graphite. The results of purifying treatments and doping experiments further demonstrated the correlation between chemical purity and erosion-resistance in the torch tests.

3. Graphite orientation played only a minor role in dynamic erosion experiments. TSX exhibited greater erosion-resistance in its poorest orientation than did the more dense ZT grades in their best directions.

4. Impregnation of relatively porous grades with either furfuryl alcohol monomer or the modified furfuryl compound, resulted in improved erosion-resistance in the dynamic erosion tests. This compound, because of its higher coke yield gave better results. It is necessary to graphitize the body after impregnation to obtain maximum improvement; mere carbonization of the impregnant

sample produced only minor changes in its firing behavior.

5. Resistance to ablation in an arc plasma test increases with higher graphite density. Ablation becomes significant at temperatures above 2600° C.

6. In contrast to results obtained in the dynamic erosion tests, there were only little differences between the oxidation rates of the various graphites either in static air to 1500° C, or in flowing atmospheres to 1900° C. Oxidative attack became progressively more superficial with oxidation at higher ambient temperatures.

7. Results of shear strength determinations on statically oxidized samples failed to reveal any correlation with the results of dynamic erosion tests, since the various graphites exhibited similar strength deterioration.

8. Samples of zirconium carbide ranging in density from 75% to 99% of the theoretical value were all severely cracked as a result of dynamic tests. Cracking occurred at the onset of the run indicating failure through thermal shock. Incorporation in ZrC of tantalum or tungsten fibers, which became carbonized during hot pressing, resulted in improved resistance to thermal spalling, although some cracking still occurred. Oxidation of ZrC did not appear to be a major problem for the dense samples.

9. ZT-4001 and two hot pressed graphite compositions exhibited virtually no erosion in the solid propellant tests. The hot pressed graphite nozzles showed considerable cracking, a result of the susceptibility of this highly anisotropic material to transverse thermal failure. Transverse cracking was more pronounced in nozzles containing graphite fibers because of the weakening effect of the oriented filaments.

10. The outstanding behavior shown by TSX in the oxy-acetylene tests was not repeated in solid propellant tests; moreover, its order of merit with respect to ZT-4001 or hot pressed graphite was reversed. Graphite density appeared to be the most important factor affecting erosion-resistance in solid propellant tests; purity was of secondary or lesser importance.

11. TSX showed slight improvement in rocket firing performance with impregnation. Impregnated ATJ samples showed fair resistance to erosion. The degree of improvement imparted by impregnants could not be evaluated since untreated ATJ was not tested. Erosion of graphite nozzles was featured by intergranular oxidative attacks.

12. Nozzles of zirconium carbide originally containing tantalum or tungsten fibers were severely cracked and eroded in the solid rocket tests. Erosion is mainly attributed to thermal spalling. Evidently, incorporation of fibers did not sufficiently improve the thermal shock-resistance of ZrC to enable it to withstand cracking in these tests. The fibers, which became carburized in hot pressing, were too brittle to act as crack stoppers or to reinforce the matrix. Oxidation of these nozzles was negligible. Coating of the nozzle throat with a thin layer of tungsten protected reinforced ZrC temporarily, although it did not prevent the substrate from cracking. The nozzle deteriorated rapidly once the coating was destroyed.

13. Thorium oxide nozzles reinforced with tungsten fibers exhibited moderately severe erosion but no gross failure. The tungsten fibers reinforced the matrix and prevented macroscopic crack formation. However, the fiber network did not prevent dislodgement of the high fractured matrix by the high-velocity gas stream. Coating of the throat with tungsten appeared to be of only temporary help. Oxidation of tungsten metal was virtually negligible.

Table I

ORIENTATION DATA BASED ON X-RAY DIFFRACTION

Grade	Longitudinal Cut		Transverse Cut		Longitudinal Cut $\frac{I_{004}}{I_{110}}$	Transverse Cut $\frac{I_{004}}{I_{110}}$	Anisotropy Factor
	I_{004}	I_{110}	I_{004}	I_{110}			
ZT-3001	222	386	818	228	0.578	3.72	0.155
	228	392	818	212			
TS-245	475	318	87	392	1.59	0.220	7.20
	465	272	84	375			

Note: The numbers represent arbitrary units of area on the diffractometer chart.

Table II

SELECTED PROPERTIES OF GRAPHITE GRADES

Grade	Fabrication Method	Mean Bulk Density g/cc	Mean Liquid Density g/cc	Per Cent Closed Porosity	Anisotropy Factor	Grain Size Relative	Pore Structure	Remarks
A. Commercial Grades								
AGSX	extruded	1.59	2.10	25	5.8	coarse	coarse	
AGSR	extruded	1.58	2.13	20	4.8	coarse	coarse	
CS	extruded	1.69	2.16	18	6.3	coarse	coarse	
AUC	extruded	1.64	2.18	13	N.D.	fine	coarse	
CCH	extruded	1.64	2.18	13	N.D.	fine	coarse	purified AUC
ATJ	molded	1.78	2.01	52	1.0	medium	medium	
B. Experimental Grades								
TS-245	extruded	1.74	2.15	21	9.0	very coarse	coarse	needle coke
TSX	extruded	1.75	2.17	10	11.5	very coarse	coarse	high-purity needle coke
RT-0003	molded	1.85	2.08	44	0.76	very coarse	medium-coarse	pressure-baked
RT-0008	molded	1.86	2.08	45	0.42	very coarse	medium-coarse	pressure-baked
ZT-2001	hot worked	1.88	2.07	50	0.20	fine	fine	
ZT-3001	hot worked	1.96	2.06	67	0.13	fine	fine	
ZT-4001	hot worked	1.90	2.07	70	0.11	fine	fine	
HPF	hot pressed	1.95*	2.01	81	0.04**	fine	fine	fabricated at ARF

* density of samples tested ranged from 1.88 to 2.01 g/cc.

** degree of anisotropy varied significantly with density of sample.

Table III

SOME MECHANICAL PROPERTIES OF HOT PRESSED GRAPHITE

	Bulk Density g/cc	Orientation	Strength psi	Elastic Modulus x 10^6 psi
A. Basic Graphite Body (90 coke, 10 thermax, 18 furfuryl alcohol)				
1. Flexural Strength	2.05	with grain	5520	
	2.05	across grain	2750	
2. Tensile Strength	2.00	with grain	2620	
3. Flexural Elastic Modulus	2.05	with grain		3.70
	2.05	across grain		0.72
4. Compressive Elastic Modulus	2.02	across grain		0.71
B. Graphite Body with Fibers (90 coke, 5 thermax, 5 graphite fibers, 20 furfuryl alcohol)				
1. Flexural Strength	1.99	with grain	5440	

Table IV

DYNAMIC EROSION DATA
(Test specimens with 0.375 inch diameter bore)

Graphite Grade	Fabrication Method	Mean Bulk Density g/cc	Mean Liquid Density g/cc	Closed Porosity %	Firing Time sec.	Per Cent Increase in Bore Volume Fuel Ratio O_2:C_2H_2		
						0.93	1.09	1.22
AUC-1*	extruded	1.59-1.63	2.14	18	3	--	2.7 ± 1.2	--
					5	--	11.5 ± 0.5	--
					7	-1.3 ± 0.3	11.9 ± 7.7	43.4 ± 2.9
					10	--	21.8 ± 3.2	--
AUC-1.25**	extruded	1.62-1.66	2.18	13	3	--	4.3 ± 2.7	--
					5	--	9.3 ± 1.1	--
					7	-2.0 ± 0.3	20.6 ± 3.3	60.6 ± 3.7
					10	--	37.9 ± 0.2	--
AGSX	extruded	1.61-1.63	2.08	28	3	--	1.7 ± 0.1	--
					5	--	6.3 ± 1.2	--
					7	-1.5 ±0.2	12.2 ± 3.3	62.0 ± 11.3
					10	--	31.4 ± 0.4	--
AGSR	extruded	1.59-1.67	2.13	20	3	--	4.3 ± 0.2	--
					5	--	10.3 ± 0.3	--
					7	-1.2 ± 0.4	19.5 ± 6.6	59.3 ± 3.0
					10	--	23.1	--
CS-112	extruded	1.61-1.66	2.15	17	3	--	3.7 ± 2.0	--
					5	--	12.2 ± 1.0	--
					7	-1.1 ± 0.2	15.4 ± 11.9	53.0 ± 7.0
					10	--	29.1 ± 0.3	--
ATJ	molded	1.76-1.78	2.02	49	5	--	9.1 ± 0.6	--
					7	2.0 ± 0.2	21.4 ± 2.4	58.2 ± 3.1
					9	--	29.8 ± 2.1	--

* samples machined from fine-grained one inch diameter stock
** samples machined from somewhat coarser, 1-1/4 inch diameter stock.

Table V

DYNAMIC EROSION DATA FOR ATJ GRAPHITE*
(Test specimens with 0.375 inch diameter bore)

Fuel Ratio O_2:C_2H_2	Firing Time mins.	Bulk Density g/cc	"Methanol" Density (unfired) g/cc	Pore Volume Inaccessible to Methanol %	"Methanol" Density (fired) g/cc	Change in Bore Volume
1.09	5	1.780	2.017	51	2.029	6.6
1.09	5	1.776	2.019	50	2.029	11.7
1.09	7	1.782	2.015	52	2.206	22.0
1.09	7	1.779	2.019	50	2.031	20.9
1.09	10	1.786	2.017	52	2.027	31.2
1.09	10	1.755	2.019	48	2.033	28.4
1.22	5	1.763	2.022	48	2.037	36.93
1.22	5	1.769	2.017	50	2.030	39.00
1.22	7	1.761	2.017	50	2.033	58.54
1.22	7	1.773	2.015	51	2.030	57.76
1.22	10	1.774	2.018	50	2.032	104.34
1.22	10	1.776	2.017	51	2.031	101.77
	Mean values	1.773	2.018	50.8		

* grain perpendicular to the bore.

Table VI

EROSION SURFACE TEMPERATURE DETERMINATIONS

Flame Condition	Fuel Ratio $O_2:C_2H_2$	Temperature Achieved at Sight Holes °C	
		T_1	T_2
	1. Specimens with 0.375 inch diameter bore		
Reducing	0.93	1600	1650
Neutral	1.09	1860	1860
Oxidizing	1.22	1940	1920
	2. Specimens with 0.250 inch diameter bore		
Neutral	1.09	1928	1926
Oxidizing	1.22	1990	1993

Table VII

DYNAMIC EROSION DATA FOR COMMERCIAL AND EXPERIMENTAL GRAPHITES
(Test specimens with 0.250 inch diameter bore; 7 minute firing duration)

Grade	Fabrication Method	Mean Bulk Density g/cc	Mean Liquid Density g/cc	Per Cent Closed Porosity	Per Cent Increase in Bore Volume	
					Neutral (1.09)	Oxidizing (1.22)
A. Commercial Grades						
AUC-1	extruded	1.64	2.18	13	38.7 ± 7.8	139.9 ± 12.8
CCH*	extruded	1.63	2.18	13	29.7 ± 6.3	84.7 ± 5.1
AGSX	extruded	1.59	2.08	26	33.8 ± 3.7	104.3 ± 7.9
AGSR	extruded	1.58	2.13	18	36.1 ± 4.8	112.3 ± 16.5
CS-112	extruded	1.62	2.15	17	25.4 ± 13.5	91.8 ± 8.8
ATJ	molded	1.73	2.01	47	25.9 ± 7.4	85.3 ± 8.9
B. Experimental Grades						
RT-0003	molded	1.85	2.08	44	26.7 ± 9.0	118.0 ± 10.0
RT-0008	molded	1.86	2.08	45	35.4 ± 8.1	115.8 ± 5.9
ZT-2001	hot worked	1.88	2.07	50	32.9 ± 6.3	115.0 ± 3.6
ZT-3001	hot worked	1.96	2.06	67	37.7 ± 6.7	124.0 ± 3.9
ZT-4001	hot worked	1.99	2.07	70	25.5 ± 8.2	110.5 ± 2.0
TS-245	extruded	1.71	2.15	21	14.7 ± 5.3	63.5 ± 9.4
TSX	extruded	1.75	2.17	18	5.5 ± 1.0	33.5 ± 0.3
HPF	hot pressed	1.95	2.01	81	41.2 ± 10.6	126.7 ± 10.1

Note: Flame parallel to grain for extruded samples and normal to grain for molded samples.
* purified AUC-1

Table VIII

CRYSTALLITE ORIENTATION DATA

Grade	Ratio of Crystallite Bases to Edges			
	Longitudinal Cut	Transverse Cut	Longitudinal Bore	Transverse Bore
ZT-3001	0.58	3.72	0.58	2.15*
TSX	2.98	0.20	2.98	1.59*

Note: A longitudinal cut is across the grain in ZT-3001 cylinders and along the grain in TSX cylinders.

* Values represent an average of those in the first two columns.

Table IX

DYNAMIC EROSION AS A FUNCTION OF ORIENTATION
(7 minute firing duration)

Grade	Fabrication Method	Anisotropy Factor	Flame Condition	Per Cent Increase in Bore Volume	
				With Grain	Across Grain
ATJ	molded	1.0	neutral	26.2	25.6
			oxidizing	79.6	95.9
ZT-3001	molded	0.13	neutral	31.9	33.1
			oxidizing	120.0	128.0
ZT-4001	molded	0.11	neutral	31.6	39.0
			oxidizing	106.3	146.8
TS-245	extruded	9.0	neutral	19.5	28.0
			oxidizing	95.2	85.7
TSX	extruded	11.5	neutral	3.8	6.2
			oxidizing	40.9	34.2

Table X

DYNAMIC EROSION STUDIES ON FLAT SAMPLES
(OXIDIZING FLAME)

Sample	Intensity Ratio of Crystallite Bases to Edges	
	With Grain	Across Grain
ZT-3001	3.72	.578
ZT-3001 (eroded)	3.37	.720
TSX	2.98	.197
TSX (eroded)	2.84	.182

Table XI

SPECTROSCOPIC ANALYSES AND RELATED DYNAMIC EROSION DATA

Graphite Grade	Impurity Content (in parts per million)								Density g/cc	Per Cent Increase in Bore Volume	
	Al	B	Ca	Fe	Mg	Si	Ti	V		Neutral Flame	Oxidizing Flame
AGSR*	10	5	1000	30	1	50	10	100	1.58	36.1	112.3
AUC*	6	1	50	20	1	30	10	50	1.64	38.7	139.9
CCH*	total impurities less than 10 ppm								1.64	29.7	84.7
ZT-3001	-	-	50	500	50	50	10	-	1.96	37.7	124.0
ZT-4001	-	-	10	500	10	50	10	-	1.99	25.5	110.5
TS-245	-	-	50	50	10	50	10	-	1.74	14.7	63.5
TSX	-	-	20	-	-	50	-	-	1.75	5.5	33.5
HPF	-	15	270	30	5	-	20	50	1.95	41.2	126.7

Note: Values reported are accurate to 10% of the figure given. Dash denotes that element was not detected.

* Average analyses for these commercial grades were furnished by National Carbon Company (data sheets SM-568H6 and 568H8).

Table XII

SPECTROSCOPIC ANALYSES AND RELATED EROSION DATA
FOR DOPED TSX SAMPLES

Doping Species	Impurity Content (in ppm)			PerCent Increase in Bore Volume	
	Ca	Fe	Ti	Neutral Flame	Oxidizing Flame
A. Control Samples					
1. TSX (untreated)	20	-	-	5.5	33.5
2. TSX (heated to 3000°C)	20	-	-	8.1	45.4
B. Doped Samples					
1. Ca	11	9	70	17.1	63.8
2. Ca, Fe	60	10	70	16.3	69.4
3. Fe	12	14	68	13.5	68.6
4. Fe, Ti	7	9	77	14.3	82.6
5. Ti	11	9	97	11.4	90.6
6. Ca, Fe, Ti	20	9	52	38.5	136.8

Note: Values reported are accurate to 10% of figure given.

Table XIII

DYNAMIC EROSION DATA ON IMPREGNATED SAMPLES

Graphite Grade	Impregnant	Bulk Density, g/cc		Liquid Density, g/cc		% Closed Porosity		% Increase in Bore Volume		
		Untreated	Impregnated	Untreated	Impregnated	Untreated	Impregnated	Untreated	Carbonized	Graphitized
AGSR	furfuryl alcohol monomer	1.65	1.75	2.13	2.04	22	42	36.1 112.3	27.0 118.6	11.2 32.5
AGSX	furfuryl alcohol monomer	1.59	1.69	2.10	2.00	24	46	33.8 104.3	28.7 99.0	11.7 44.8
ATJ	furfuryl alcohol monomer	1.75	1.81	2.01	1.99	48	61	25.6 95.9	16.5 96.4	6.3 27.6
AUC-1	furfuryl alcohol monomer	1.64	1.71	-	-	-	-	38.7 139.9	- -	18.2 79.9
AUC-1	modified furfuryl compound	1.64	1.80	-	-	-	-	38.7 139.9	- -	15.3 49.1
TS-245	furfuryl alcohol monomer	1.74	1.79	2.15	1.99	21	57	14.7 63.5	- -	11.8 63.0
TSX	furfuryl alcohol monomer	1.75	1.89	2.17	2.06	19	54	5.5 33.5	- -	8.1 36.8

Note: Upper erosion value for each grade was obtained under neutral conditions and lower value, under oxidizing conditions.

Table XIV

ARC-PLASMA EROSION DATA

Graphite Grade	Fabrication Method	Bulk Density g/cc	Approximate Surface Temperature, °C	Per Cent Increase in Bore Volume
TSX	extruded	1.75	2900 - 3000	21.2
AGSX	extruded	1.59	2900 - 3000	38.3
RT-0008	molded	1.86	2700 - 2900	17.2
ZT-3001	molded	1.90	2700 - 2900	16.5
ATJ	molded	1.75	2900 - 3000	25.9

Table XV

STATIC OXIDATION DATA
(Small Tube Furnace)

Graphite Grade	Bulk Density g/cc	Liquid Density g/cc	Closed Porosity*	Oxidation Rate % Weight Loss Per Minute			Liquid Density of Fired Sample g/cc		
				1000°C	1250°C	1500°C	1000°C	1250°C	1500°C
A. Commercial Grades									
AGSX	1.60	2.10	24	0.27	0.29	0.30	2.22	2.17	2.16
AGSR	1.59	2.13	19	0.26	0.35	0.29	2.21	2.16	2.16
ATJ	1.78	2.01	53	0.29	0.23	0.23	2.13	2.08	2.07
CS	1.68	2.16	17	0.22	0.25	0.27	2.16	2.16	2.19
AUC-1	p.62	2.19	11	0.13	0.19	-	2.22	2.20	-
B. Experimental Grades									
RT-0003	1.85	2.09	43	0.17	0.20	0.28	2.13	2.10	2.09
RT-0008	1.86	2.08	45	0.18	0.23	0.27	2.12	2.09	2.09
ZT-2001	1.89	2.07	51	0.16	0.19	0.27	2.11	2.09	2.07
ZT-3001	1.90	2.06	56	0.17	0.21	0.27	2.11	2.08	2.09
ZT-4001	1.96	2.08	62	0.18	0.20	0.29	2.10	2.09	2.08
TS-245	1.74	2.15	21	0.17	0.23	0.27	2.21	2.21	2.17
TSX	1.75	2.17	19	0.20	0.22	0.26	2.21	2.20	2.17

* Porosity inaccessible to methanol.

Table XVI

STATIC OXIDATION DATA
(Large Globar Furnace)

Graphite Grade	Bulk Density g/cc	Liquid Density g/cc	% Closed Porosity	Oxidation Rate % Weight Loss per Minute		Liquid Density of Fired Samples	
				1000°C	1500°C	1000°C	1500°C
ZT-3001	1.90	2.06	56	0.78	0.85	2.09	2.08
ZT-4001	1.96	2.08	62	0.77	0.95	2.10	2.08
TS-245	1.74	2.15	21	0.78	0.97	2.19	2.17
TSX	1.75	2.17	19	0.69	0.79	2.20	2.17

Table XVII

OXIDATION DATA - FLOWING ATMOSPHERES

Graphite Grade	Oxidation Rates at Different Gas Flow Rates (% wt. loss per min.)				Liquid Density Oxidized Samples g/cc	Temperature, °C
	0.15 /min.	0.57 /min.	0.83 /min.	1.06 /min.		
A. Pure Oxygen Gas						
ZT-3001		13.9	15.1	15.7	2.06	Graphite Surface:
ZT-4001		14.2	15.8	16.0	2.07	0.57 /min, 1700
TS-245		14.4	16.0	16.5	2.16	0.83 /min, 1730-1750
TSX		14.3	15.4	16.2	2.17	1.06 /min, 1750-1770
TSX (doped with Ca, Fe, Ti)		14.6	15.9	16.4	-	Ambient: 1650
B. Carbon Dioxide						
ZT-3001	3.3	4.8	5.0	-	-	Graphite Surface:
ZT-4001	3.5	4.6	4.8	-	-	0.15 /min, 1510-1550
TS-245	3.7	5.0	5.2	-	-	0.57 /min, 1500-1520
TSX	3.3	4.7	5.0	-	-	0.83 /min, 1505-1515
						Ambient: 1605-1610
C. Dry Air						
ZT-3001	2.4	3.7	4.6	-	2.07	Graphite Surface:
ZT-4001	-	4.2	4.3	5.0	2.07	0.15 /min, 1570-1600
TS-245	2.9	4.0	4.5	-	2.16	0.57 /min, 1610-1615
TSX	2.4	3.9	4.3	-	2.17	0.83 /min, 1620-1625
						Ambient: 1645-1650

Table XVIII

SHEAR STRENGTH OF OXIDIZED SAMPLES

Graphite Grade	Orientation with Respect to Grain	Untreated Shear Modulus psi	Oxidized in Air at 1000°C for 30 min.			Oxidized in Air at 1500°C for 30 min.		
			Oxidation Rate % wt. loss per min.	Shear Modulus psi	% Decrease in Shear Modulus	Oxidation Rate % wt. loss per min.	Shear Modulus psi	% Decrease in Shear Modulus
ZT-3001	across	1499	0.79	854	43.0	1.54	1000	33.5
	with	1526	0.75	899	41.0	1.00	1130	26.0
ZT-4001	across	1405	0.85	724	48.4	1.43	927	34.2
	with	1297	0.08	783	39.6	1.29	885	31.8
TS-245	across	1255	0.85	692	44.8	1.24	697	44.4
	with	1025	0.70	731	28.8	1.05	703	31.6
TSX	across	915	0.69	853	6.9	1.13	669	26.9
	with	965	0.67	746	22.7	1.24	673	30.3

Table XIX

DYNAMIC TEST DATA ON ZIRCONIUM CARBIDE

Composition	Source	Density g/cc	% Theoretical Value	Flame	Remarks
A. Unreinforced Zirconium Carbide					
ZrC	ARF	4.50	67	neutral	severely cracked and oxidized
ZrC	ARF	4.51	67	oxidizing	severaly cracked and oxidized
ZrC	ARF	5.98	89	neutral	severely cracked
ZrC	ARF	6.10	91	oxidizing	severely cracked
ZrC	Carborundum	6.58	98	neutral	severely cracked
ZrC	Carborundum	6.65	99	oxidizing	severely cracked
B. Reinforced Zirconium Carbide					
ZrC + 25 w/o W fibers	ARF	5.95	75	oxidizing	some cracking
ZrC + 25 w/o W fibers	ARF	6.12	77	neutral	uncracked
ZrC + 17 w/o Ta fibers	ARF	5.60	74	oxidizing	uncracked at first, but developed cracks when quenched in water
ZrC + 17 w/o Ta fibers	ARF	5.64	74	neutral	uncracked

Table XX

MATERIALS USED IN SOLID PROPELLANT TESTS

Sample Designation	Material	Density g/cc	Apparent Porosity %	Remarks
AA-1	Hot pressed graphite	1.97	5.6	
AA-2	Hot pressed graphite	1.96	5.6	
BB-1	Untreated TSX graphite (National Carbon Co.)	1.72	20.5	
BB-2	Untreated TSX graphite (National Carbon Co.)	1.71	20.5	
CC-1	Zirconium carbide-tungsten fibers	5.88	24.8	small crack in entrance cone
CC-2	Zirconium carbide-tungsten fibers	6.08	22.8	small crack in entrance cone
DD-1	Zirconium carbide-tantalum fibers	5.88	22.9	
DD-2	Zirconium carbide-tantalum fibers	6.02	20.0	
EE-1	Thorium oxide-tungsten fibers	10.69	1.0	
EE-2	Thorium oxide-tungsten fibers	10.75	0.8	small crack in throat
FF-1	Hot pressed graphite-graphite fibers	1.98	3.8	
FF-2	Hot pressed graphite-graphite fibers	1.97	4.9	
GG-1	ZT-4001 graphite (National Carbon Co.)	2.00	0.8	
GG-2	ZT-4001 graphite (National Carbon Co.)	2.00	1.4	
HH-1	TSX graphite imprg. with furfuryl compound	1.86	9.9	
HH-2	TSX graphite imprg. with furfuryl compound	1.87	9.6	
II-1	ATJ graphite imprg. with furfuryl compound	1.75	11.1	
II-2	ATJ graphite imprg. with furfuryl compound	1.69	12.3	
JJ-1	ATJ graphite imprg. with furfuryl compound	1.74	12.3	
JJ-2	ATJ graphite imprg. with furfuryl compound	1.74	11.9	
KK-2	Zirconium carbide-tungsten fiber-tungsten coating	-	-	radial crack in nozzle and coating
LL-2	Thorium oxide-tungsten fiber-tungsten coating	-	-	

Table XXI

SOLID PROPELLANT FIRING DATA

Sample Designation	Material	Propellant	Maximum Chamber Pressure psi	Increase in Throat Area, %		Remarks
				Measured*	Calculated**	
AA-1	Hot pressed graphite	Thiokol	690	0.8	-0.2	transverse cracks
AA-2	Hot pressed graphite	Hercules	600	0.6	-1.0	several cracks
BB-1	Untreated TSX	Thiokol	730	2.8	6.7	uncracked
BB-2	Untreated TSX	Hercules	570	6.2	5.0	uncracked
CC-1	ZrC-W fibers	Thiokol	580	74.3	78.3	severe erosion and cracking
CC-2	ZrC-W fibers	Hercules	460	-	81	severe erosion and cracking
DD-1	ZrC-Ta fibers	Hercules	400	-	96	severe erosion and cracking
DD-2	ZrC-Ta fibers	Thiokol	590	70.8	67.6	severe erosion and cracking
EE-1	ThO_2-W fibers	Hercules	420	-	65	moderately severe erosion, no large cracks
EE-2	ThO_2-W fibers	Thiokol	530	46.1	60.8	moderately severe erosion, some fine cracks
FF-1	H.P. graphite-graphite fibers	Hercules	590	1.3	0.4	transverse cracks
FF-2	H.P. graphite-graphite fibers	Thiokol	610	-3.2	-2.0	transverse cracks
GG-1	ZT-4001	Hercules	570	-4.3	-0.7	uncracked
GG-2	ZT-4001	Thiokol	670	0.9	-1.0	uncracked
HH-1	TSX impr. with modified furfuryl compound	Hercules	570	5.8	4.0	uncracked
HH-2	TSX impr. with modified furfuryl compound	Thiokol	670	4.3	0.5	uncracked
II-1	ATJ impr. with modified furfuryl compound	Hercules	600	6.3	5.0	uncracked
II-2	ATJ impr. with modified furfuryl compound	Thiokol	690	3.4	0.5	uncracked
JJ-1	ATJ impr. with furfuryl alcohol	Hercules	580	1.1	1.0	uncracked
JJ-2	ATJ impr. with furfuryl	Thiokol	740	4.7	-1.0	uncracked
KK-2	ZrC-W fibers-W coating	Thiokol	520	24.5	26.2	moderately severe erosion, severely cracked
LL-2	ThO_2-W fibers-W coating	Thiokol	440	21.3	29.1	moderately severe erosion, no large cracks

* Determined from shadowgraphs and planimeter measurements.

** Calculated from chamber pressure curves.

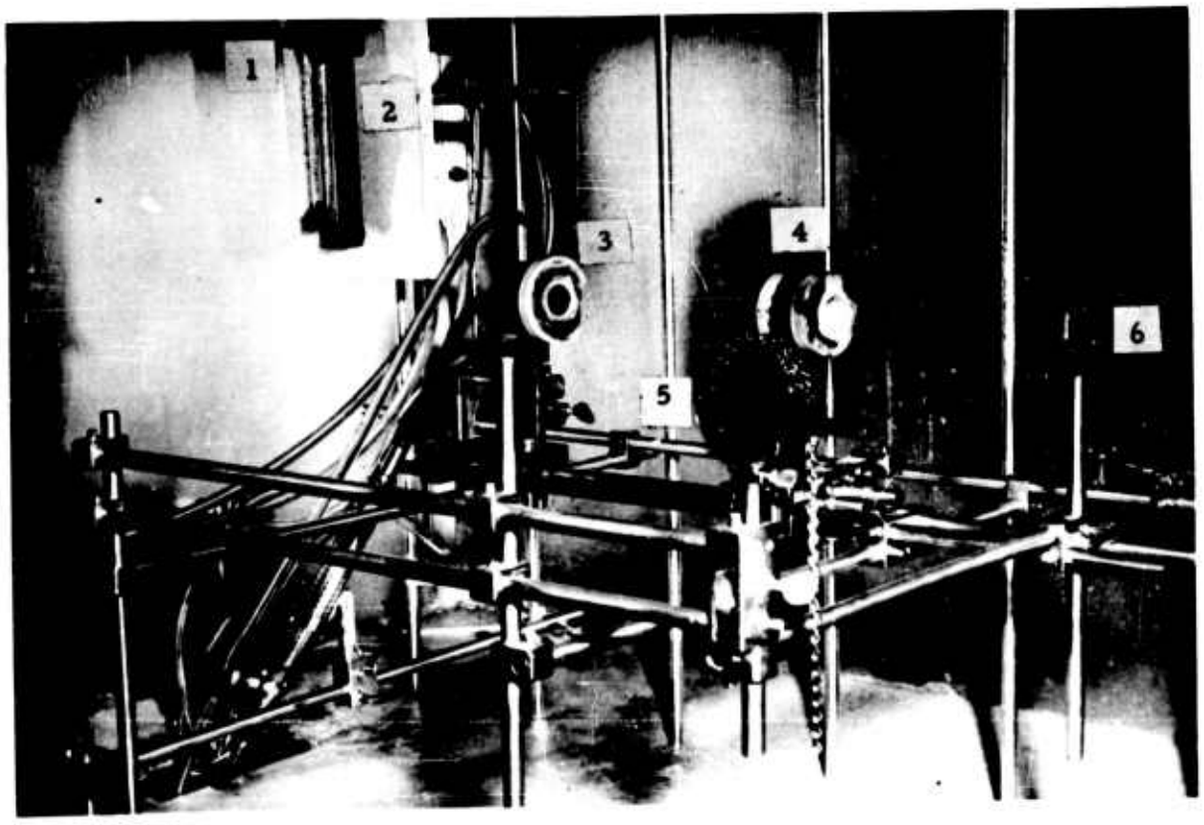

1. Flowmeter for acetylene gas
2. Flowmeter for oxygen gas
3. Torch assembly
4. Specimen holder assembly
5. Holder for optical pyrometer (Leeds and Northrup)
6. Prism

Figure 1 - Erosion Test Apparatus

Model I

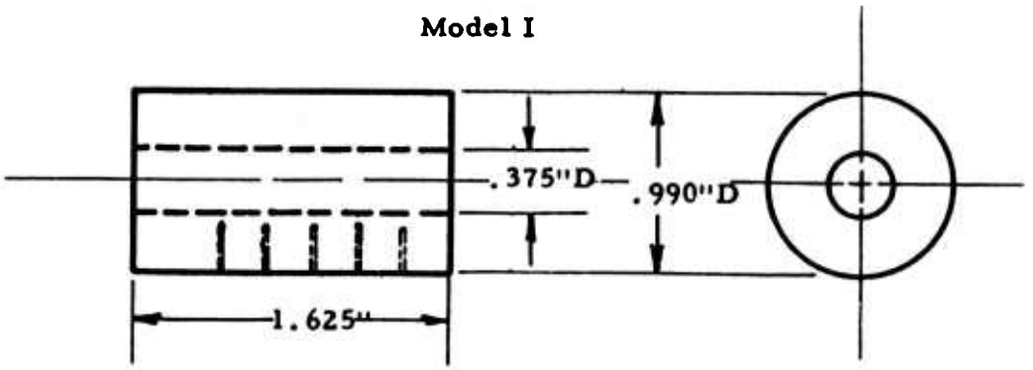

Model II

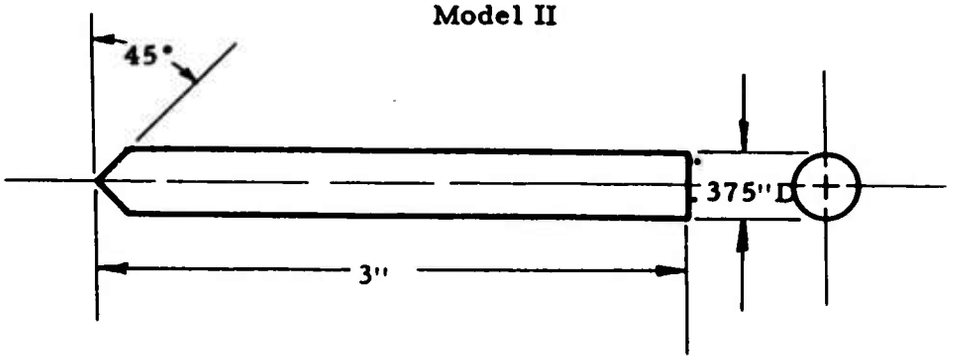

Model III

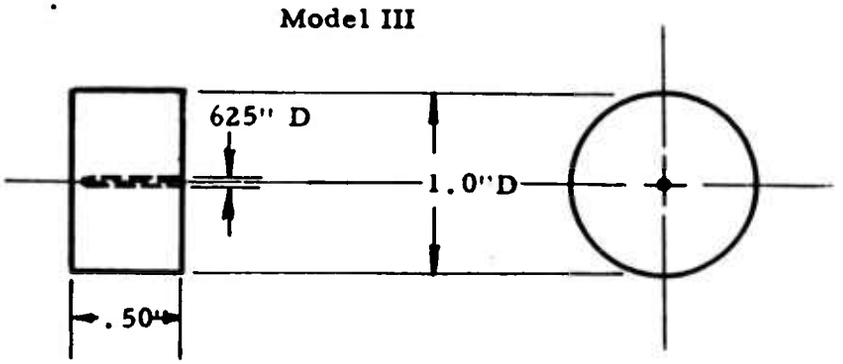

Figure 2 - Diagrams of models

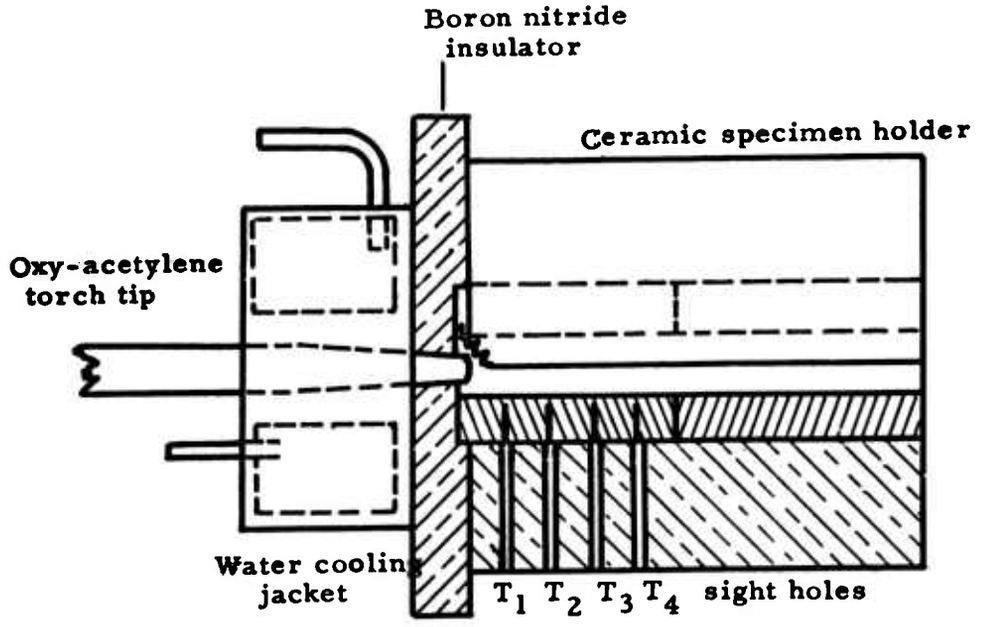

Erosion test assembly for thick-wall cylinder - top view

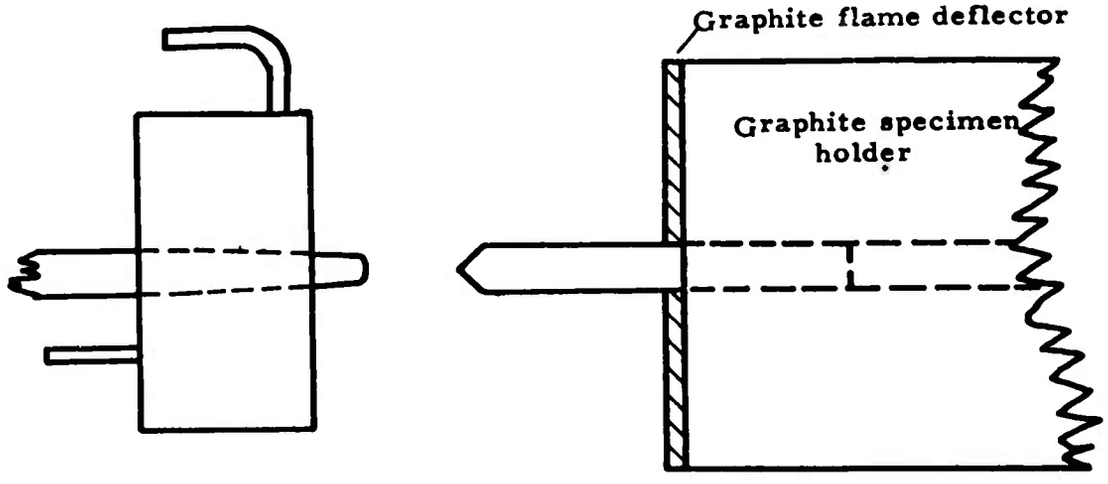

Erosion test assembly for graphite rod - top view

Figure 3 - Diagrams of flame attack
and specimen holder assembly

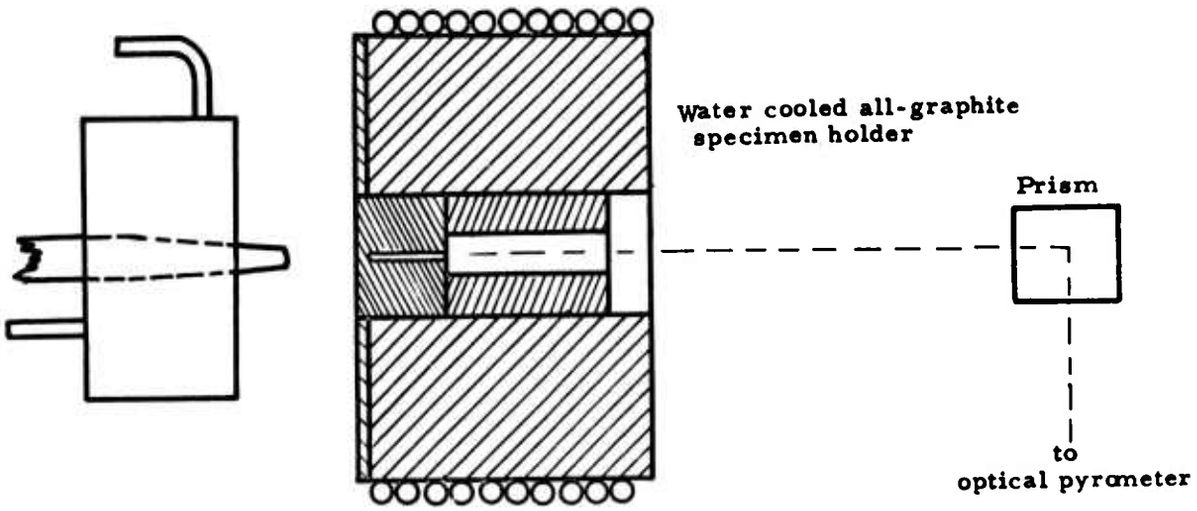

Flame attack normal to specimen surface - side view

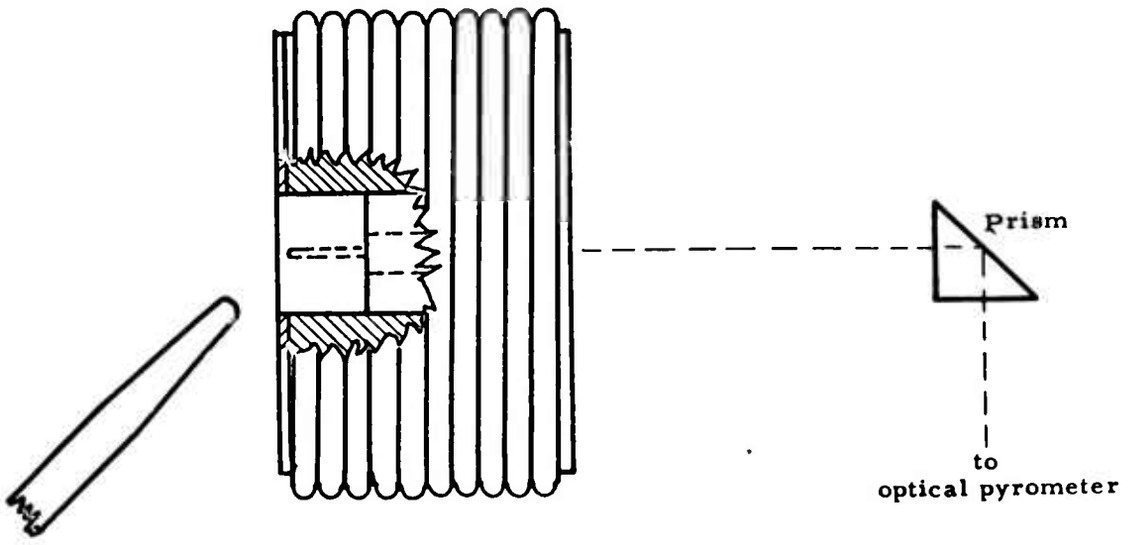

45° angle flame attack - top view

Figure 4 - Diagrams of flame attack on disk-shaped specimen

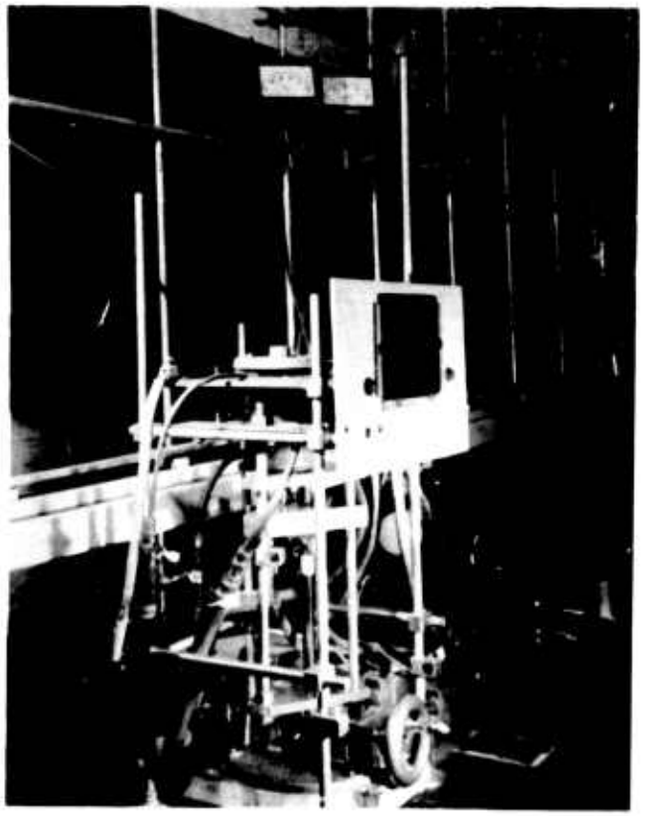

Figure 5 - Arc Plasma Erosion Apparatus

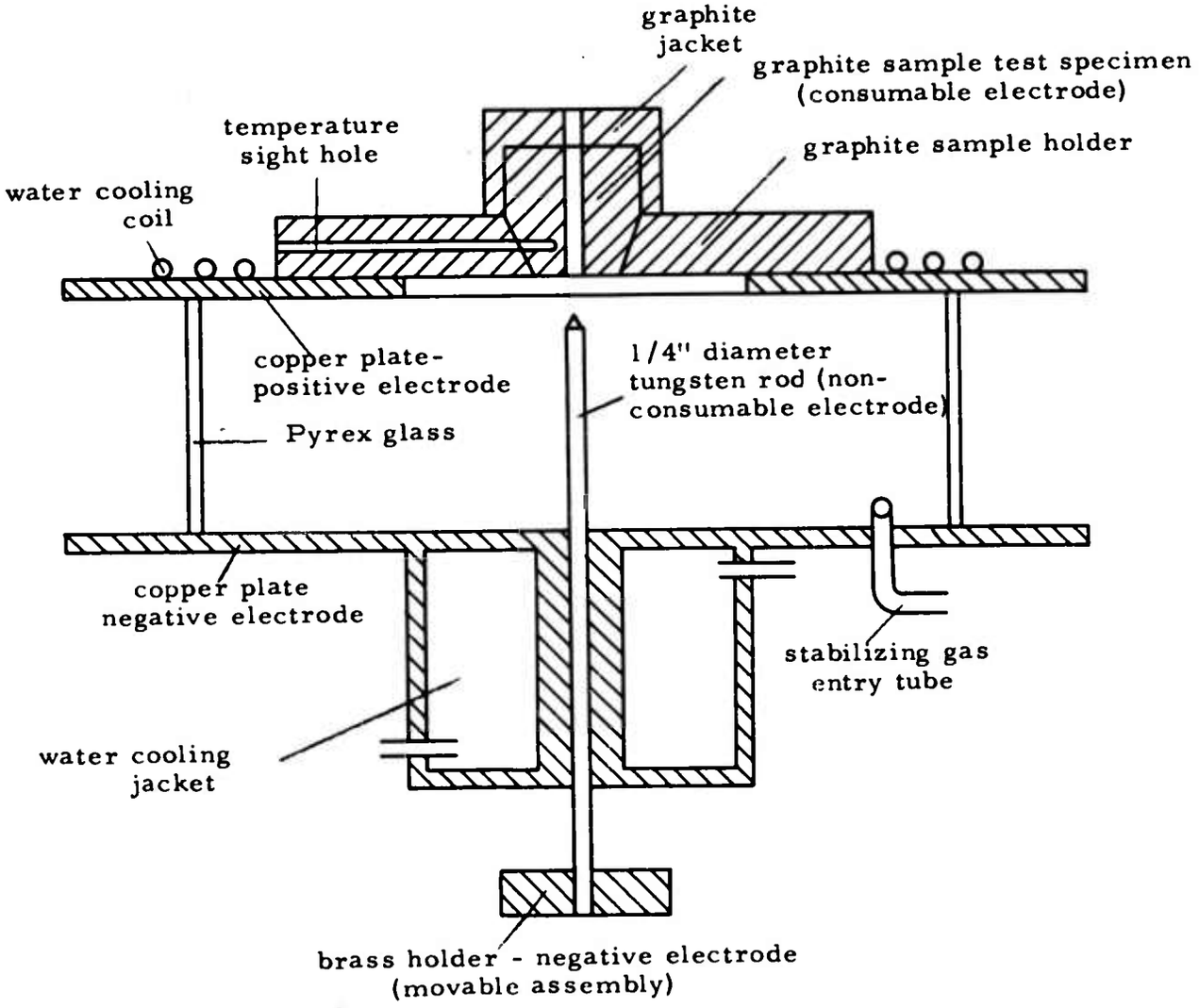

Figure 6a - Half-view of arc plasma unit (electrode section)

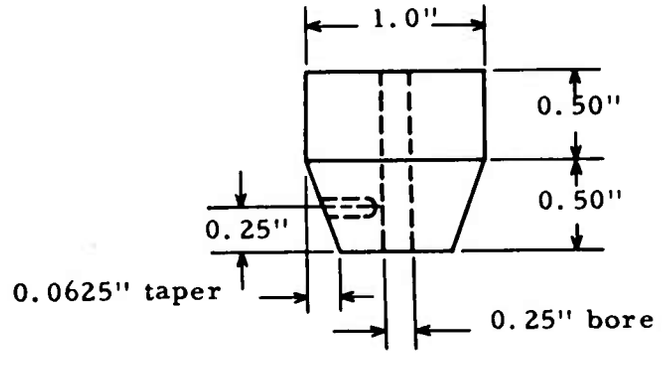

Figure 6b - Dimensions of an arc plasma test specimen

Figure 7 - Unfired RT-0003, X150

Figure 8 - Unfired RT-0008, X150

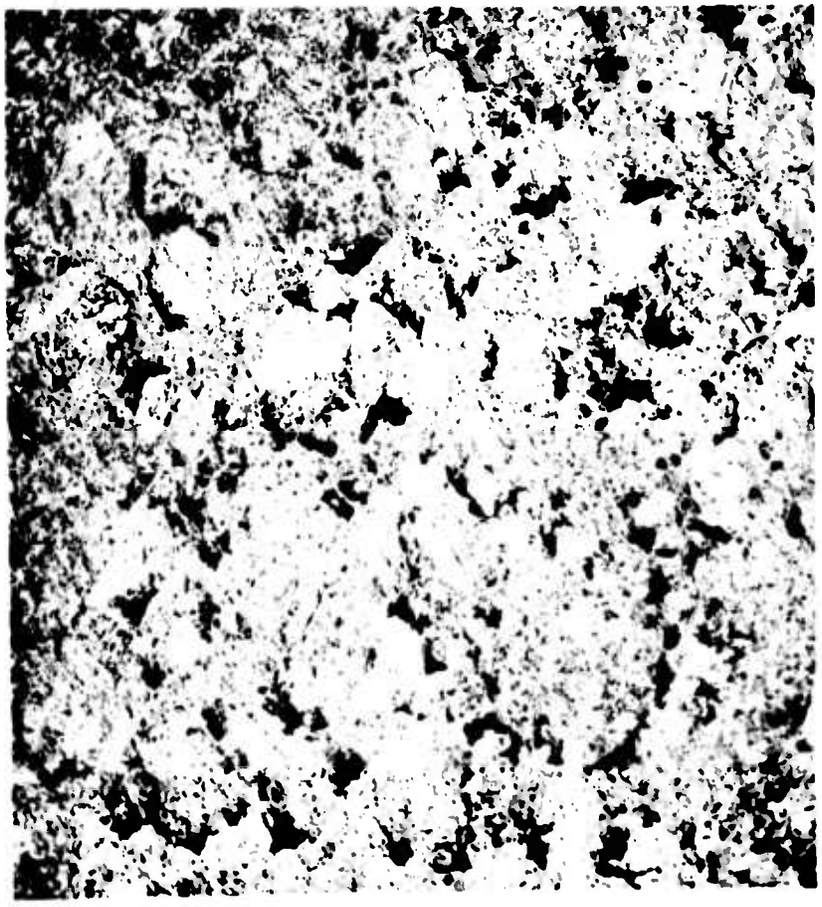

Figure 9 - Unfired ZT-3001, X150

Figure 10 - Unfired ZT-4001, X150

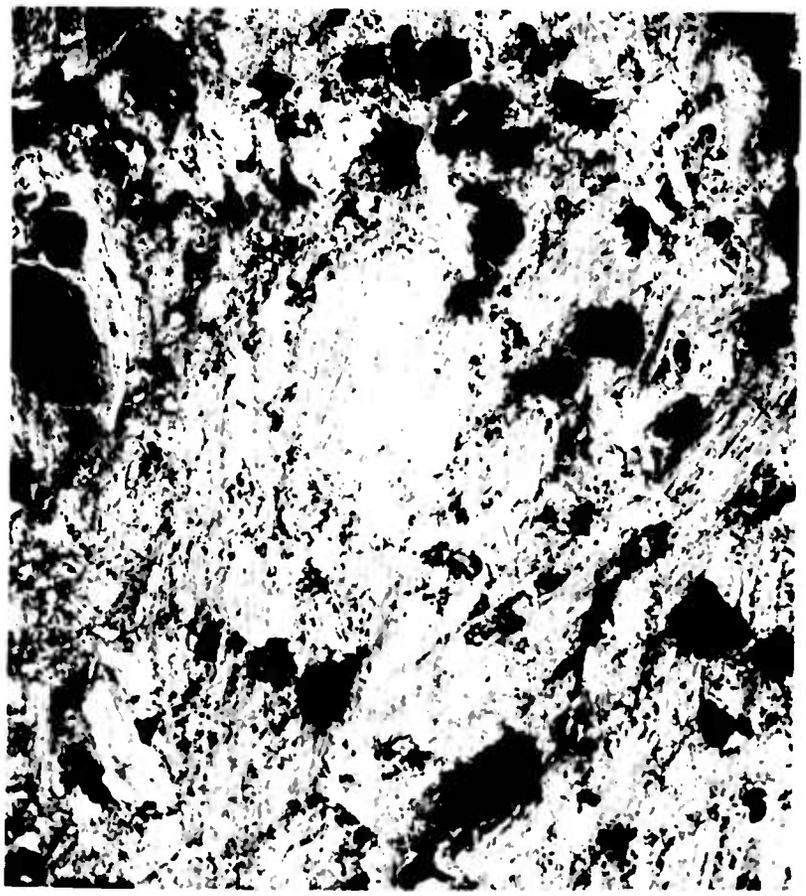

Figure 11 - Unfired TS-245, X150

Figure 12 - Unfired TSX, X150

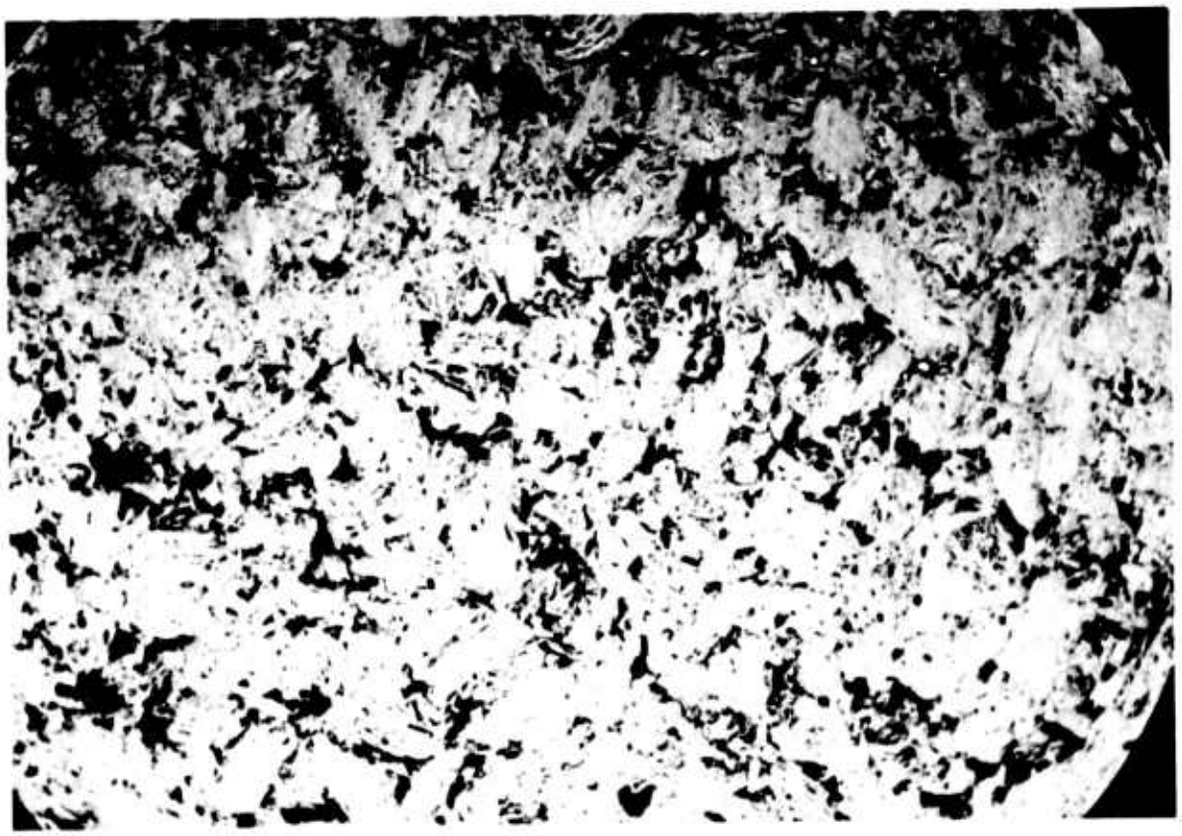

Figure 13 - Hot Pressed Graphite
Density, 1.81 g/cc, (X150)

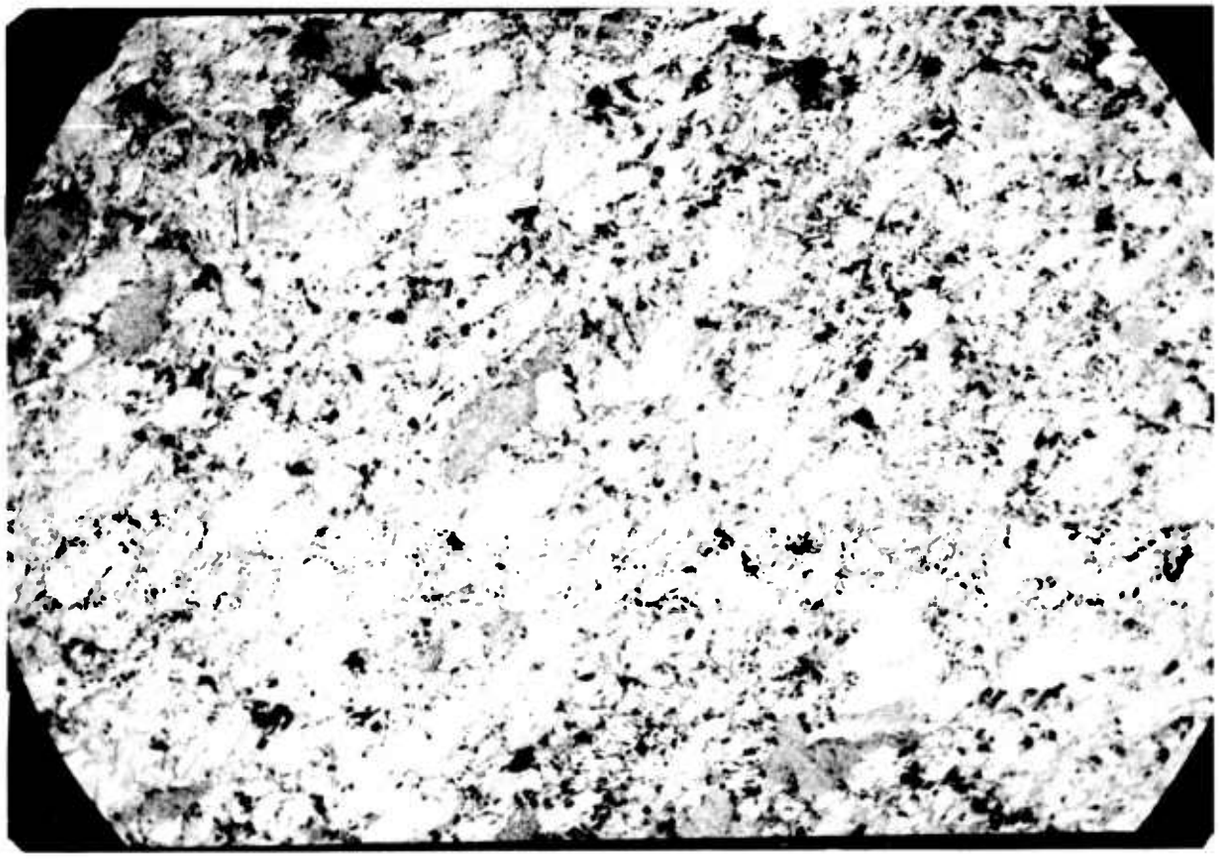

Figure 14 - Hot Pressed Graphite, Density 2.05 g/cc.
Grain trends from lower left to upper right.
X150

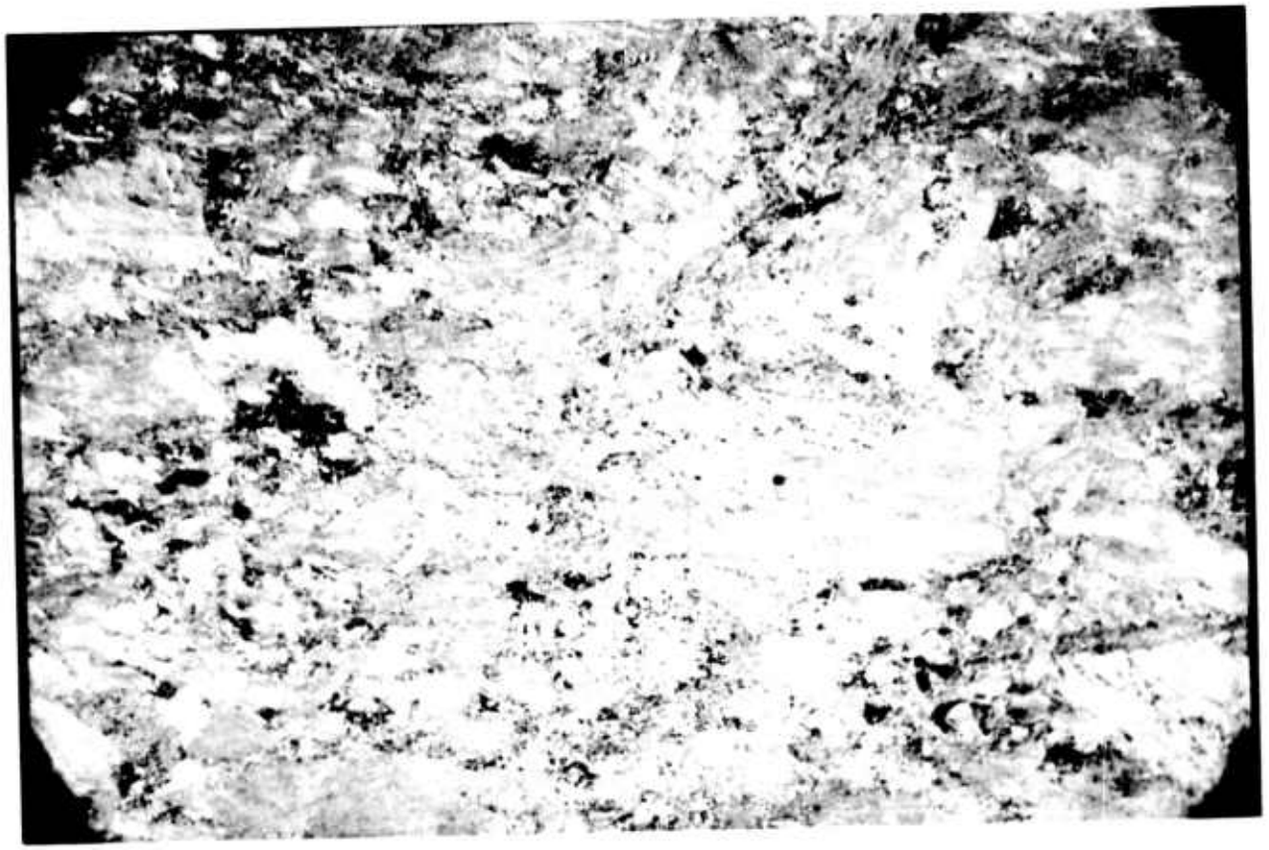

Figure 15 - Same Hot Pressed Graphite.
Grain is horizontal. X500

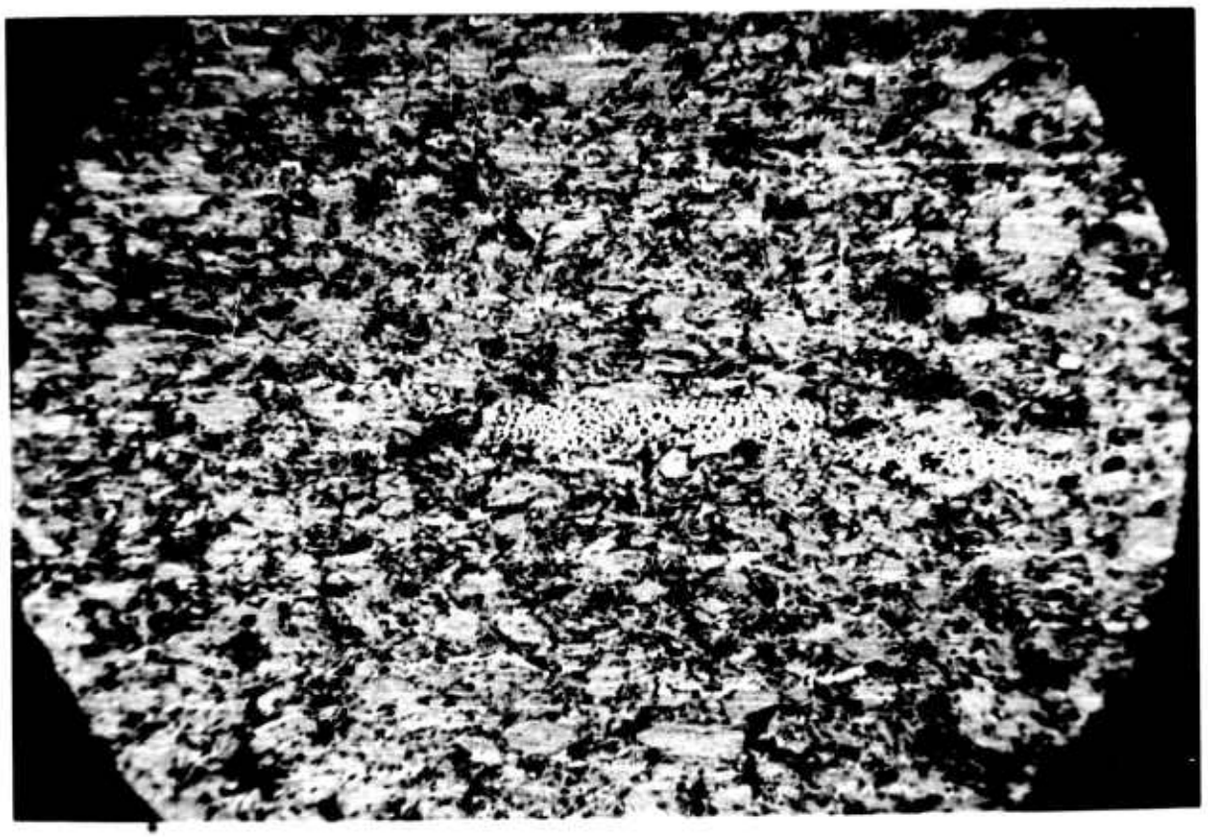

Figure 16 - Hot Pressed Graphite Containing Graphite Fibers (fragment of cloth that did not break up is seen in center). X150

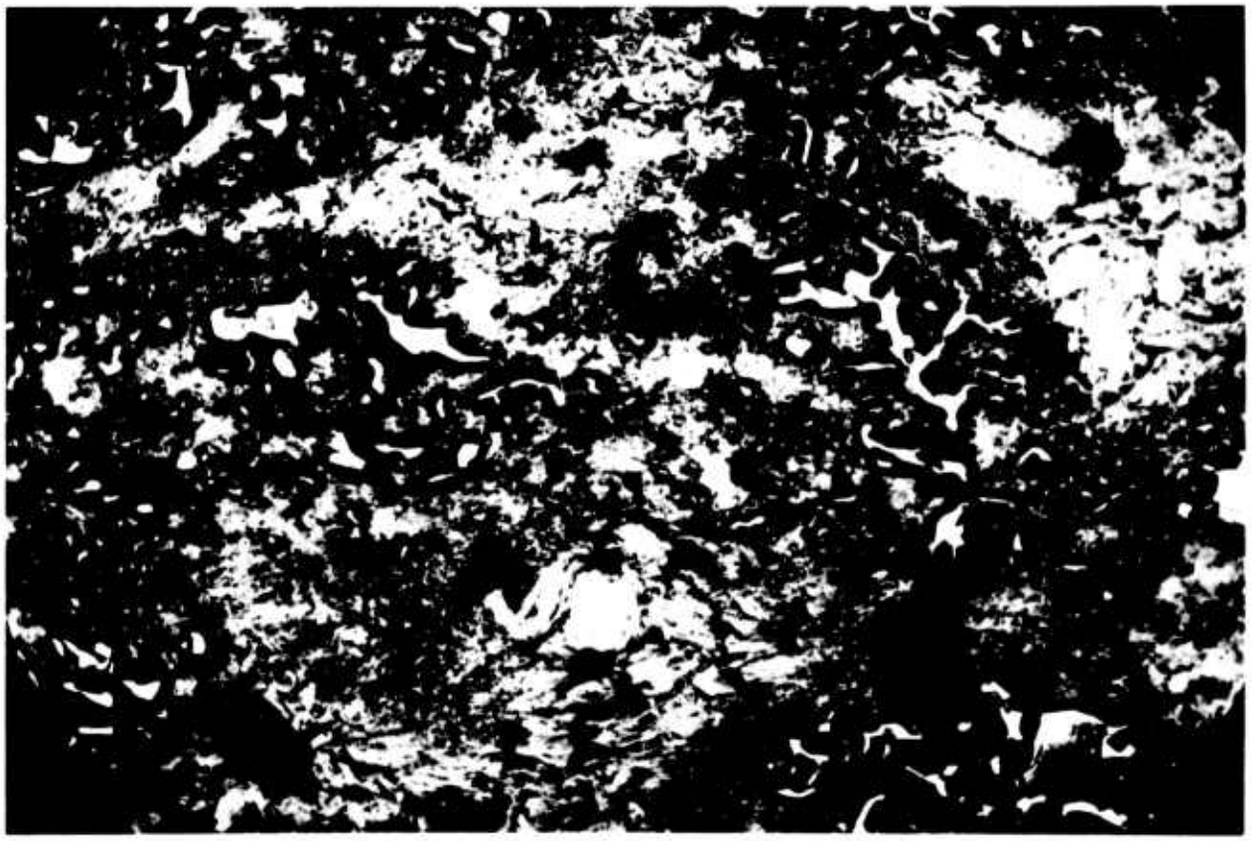

Figure 17 - Hot Pressed Graphite with 10 w/o Tungsten Fibers. Bright areas represent tungsten carbide trapped in pores in the graphite. X150

Figure 18 - Hot Pressed Graphite with 10 w/o Tantalum Fibers.
Bright areas represent tantalum carbide. X150

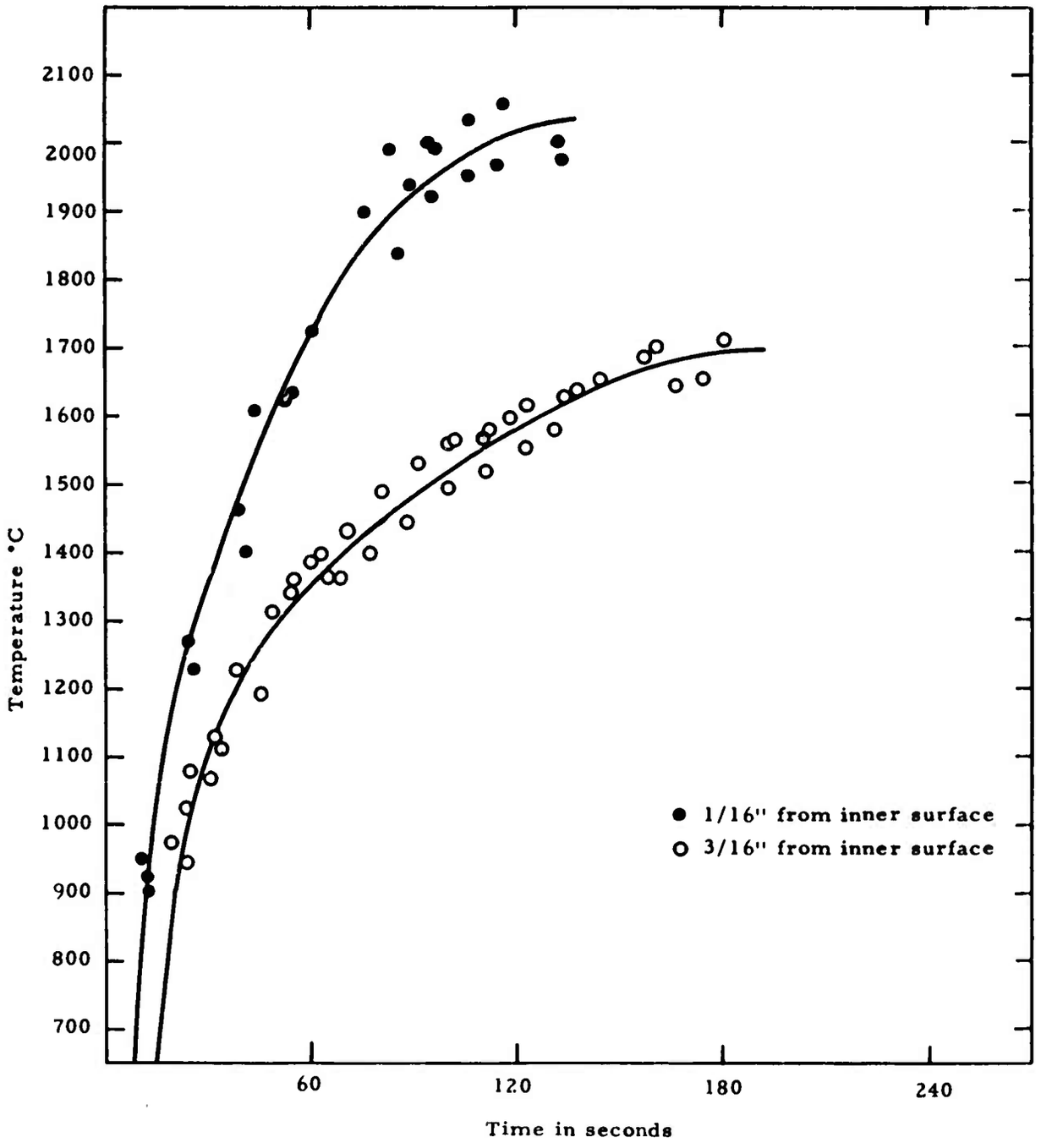

Figure 19 - Rate of heating at two different sites in the cylinder (T_2 sight hole)

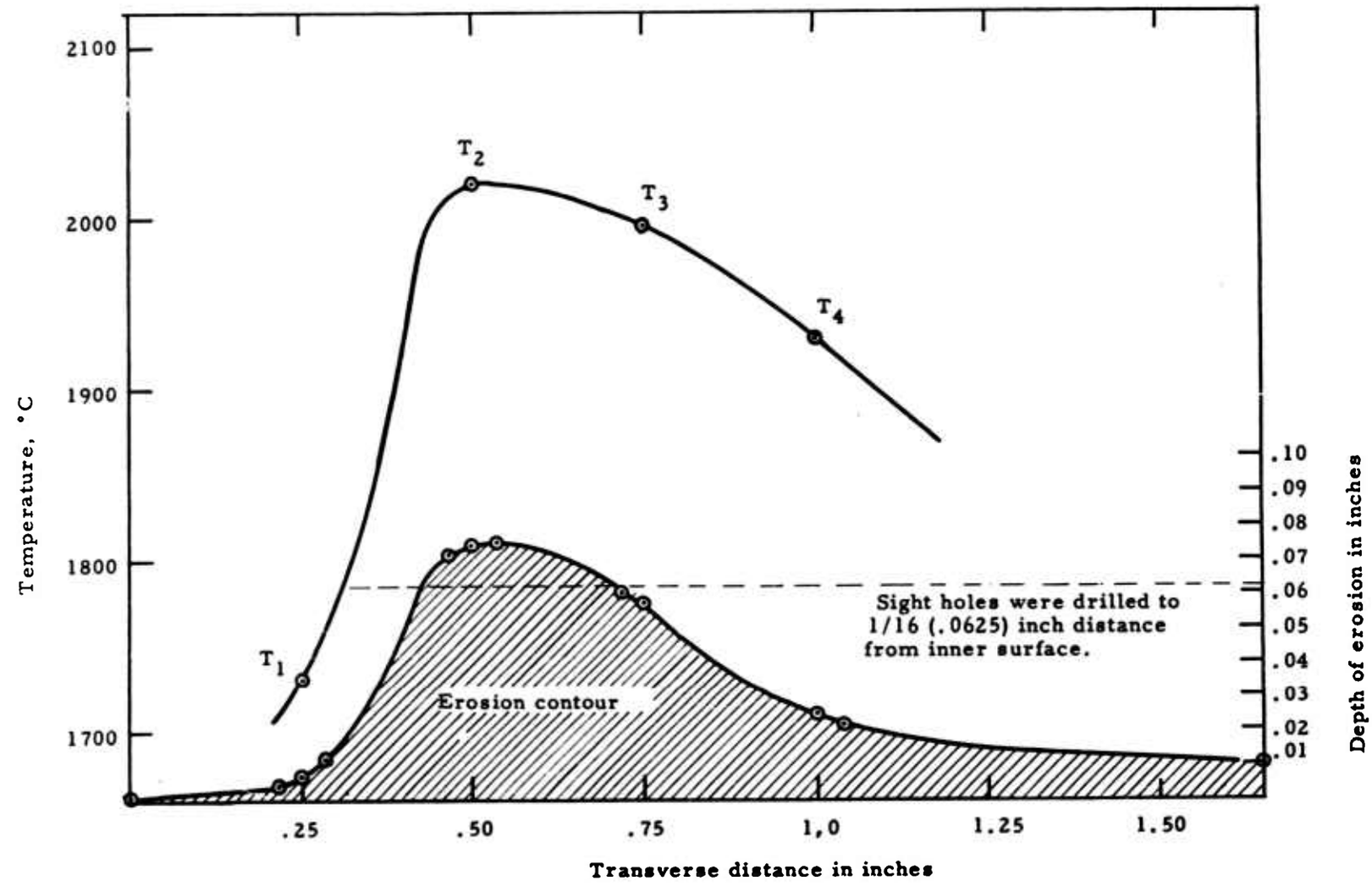

Figure 20 - Composite plot of transverse temperature and erosion profiles for Model I configuration - Speer 250 extruded graphite. Duration of fire: 3 minutes.

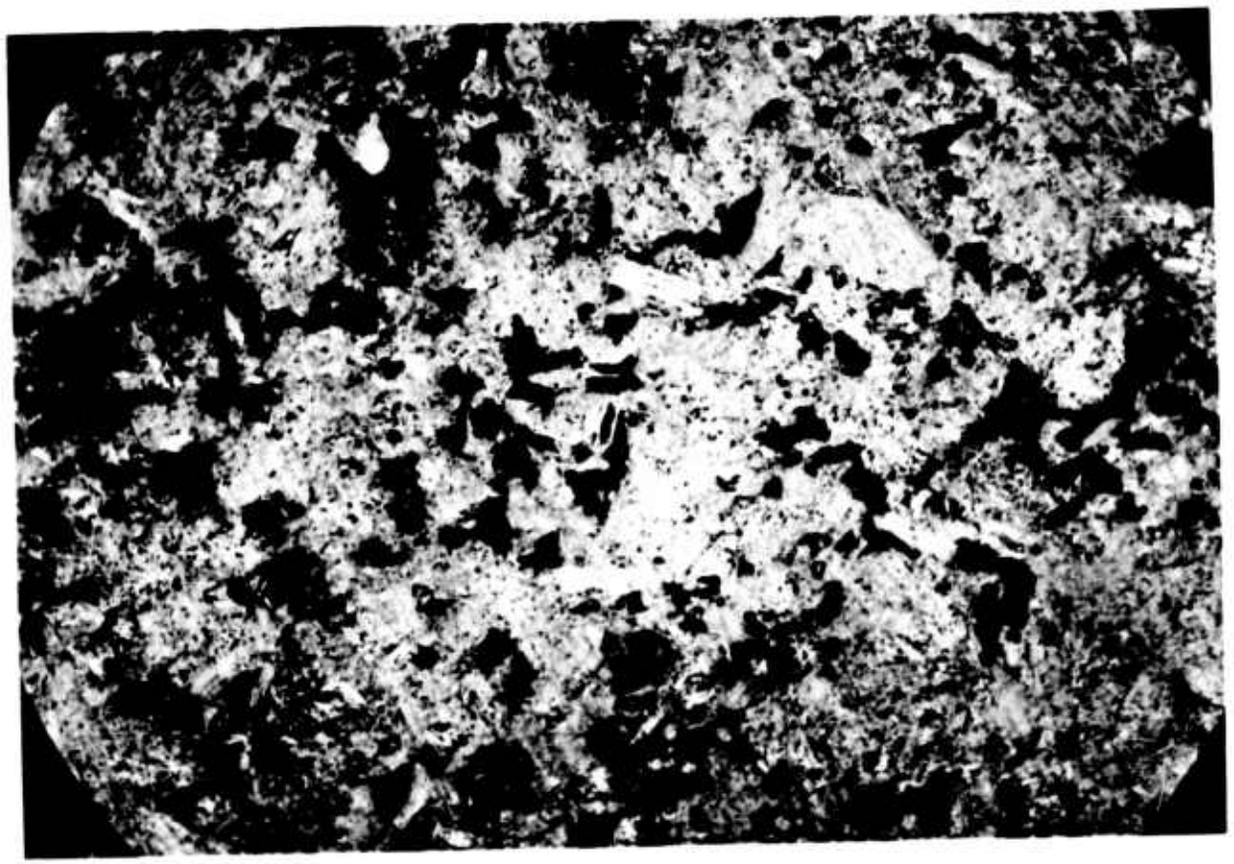

Figure 21 - Unfired ATJ, X150

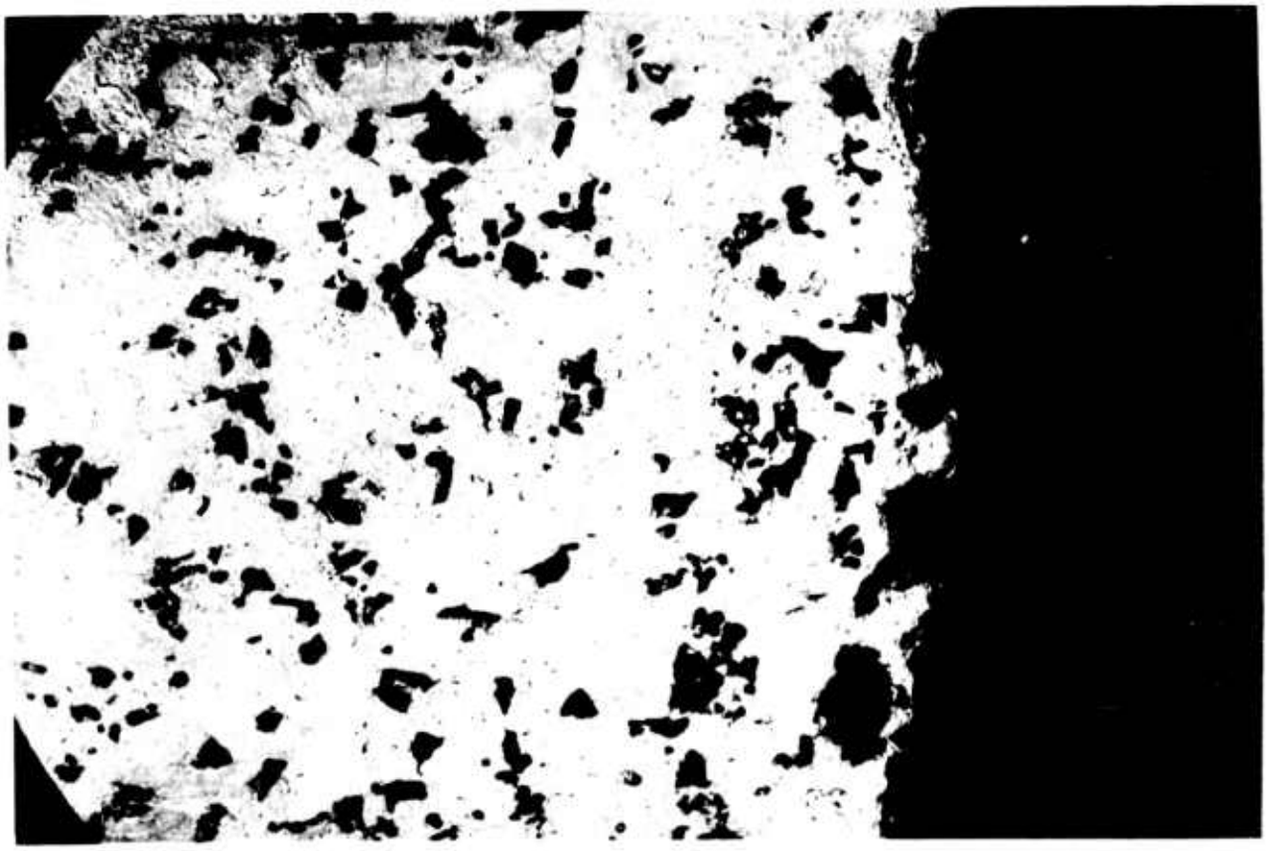

Figure 22 - Fired ATJ. Subjected to oxidizing flame for seven minutes. X150

Figure 23 - TSX Impregnated with
Furfuryl Alcohol and Baked at 3000°C.
X150

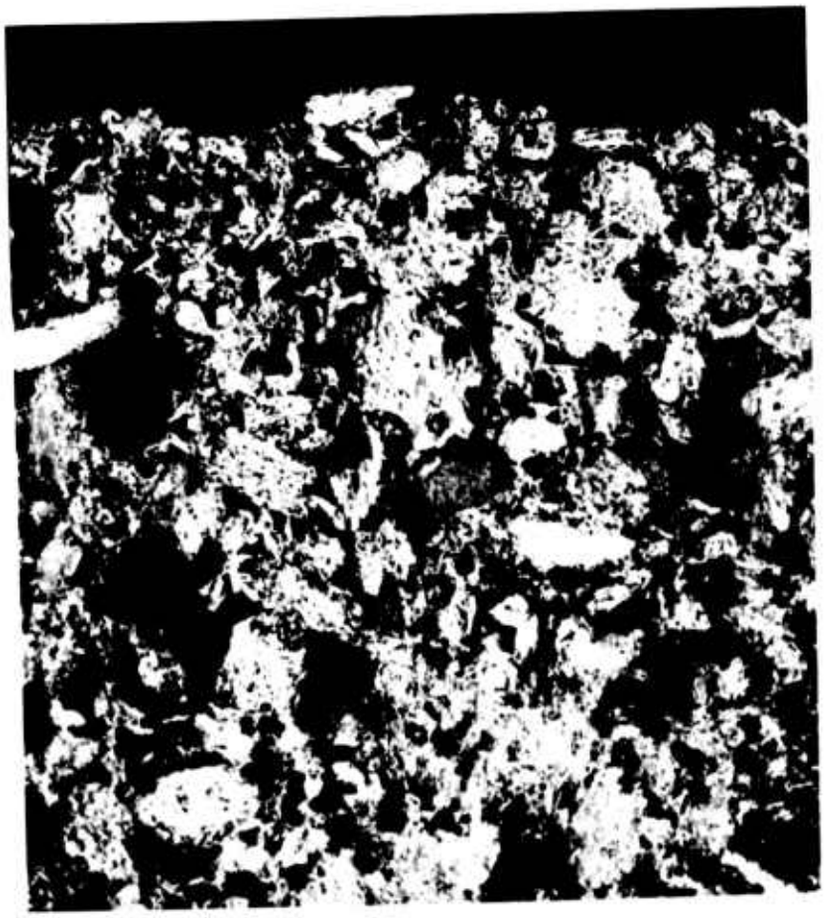

Figure 24 - ATJ Oxidized in Air at 1000°C for 105 Minutes, X150

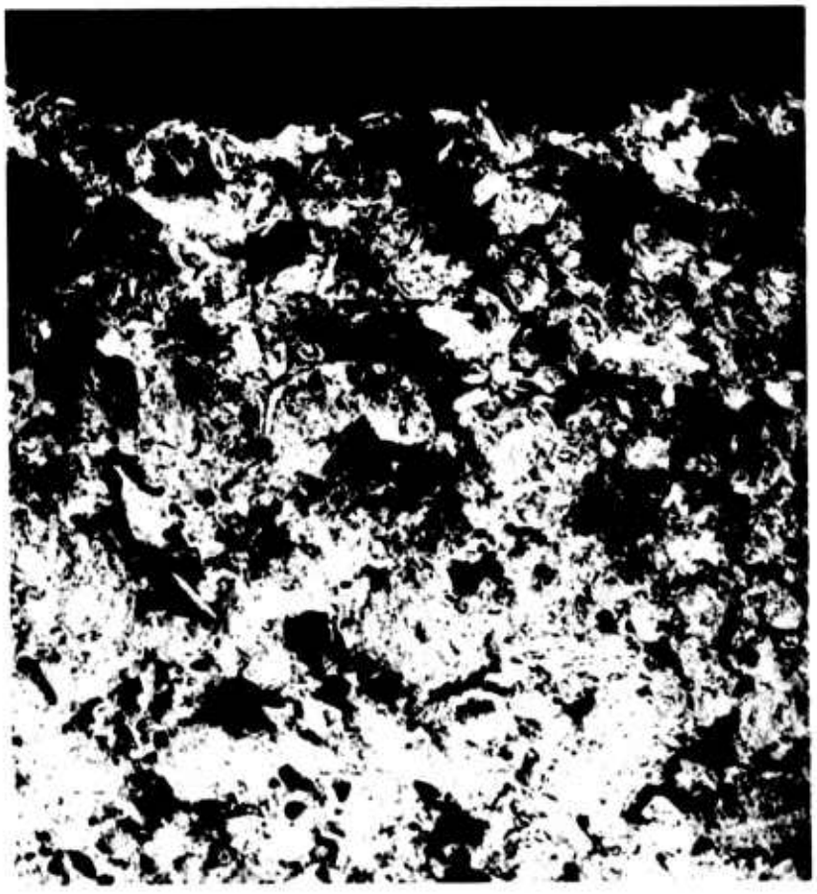

Figure 25 - ATJ Oxidized in Air at 1250°C for 105 Minutes.
X150

Figure 26 - ATJ Oxidized in Air at 1500°C for 105 Minutes, X150

Figure 27 - Unfired Zirconium Carbide (Armour), Density 4.81 g/cc, X150

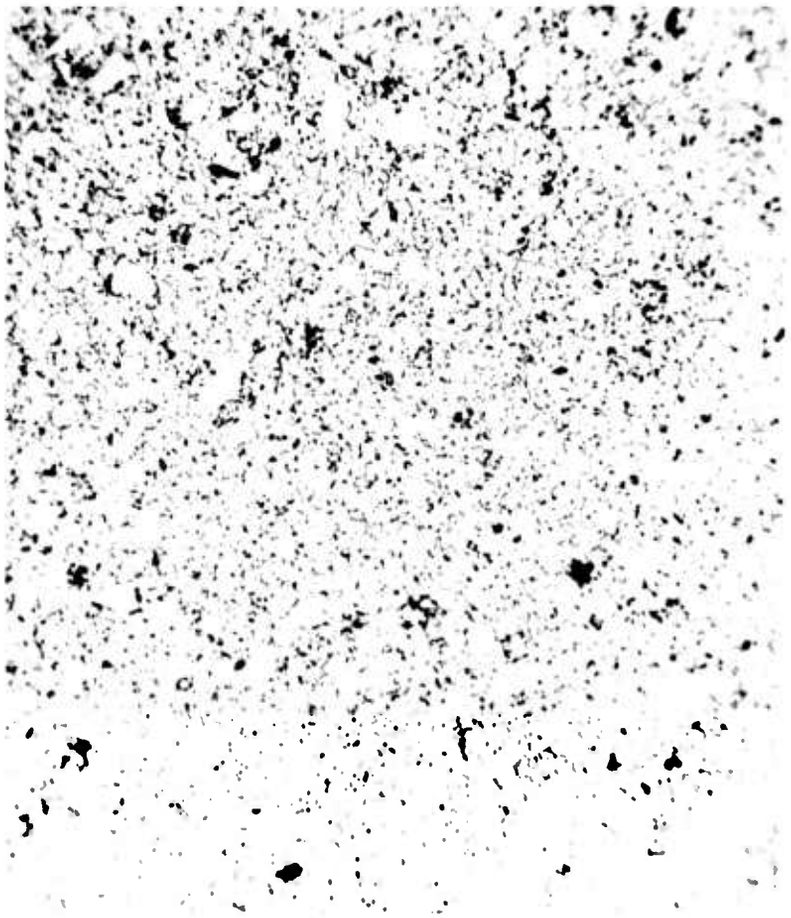

Figure 28 - Unfired Zirconium Carbide (Armour), Density 6.04 g/cc, etched X150

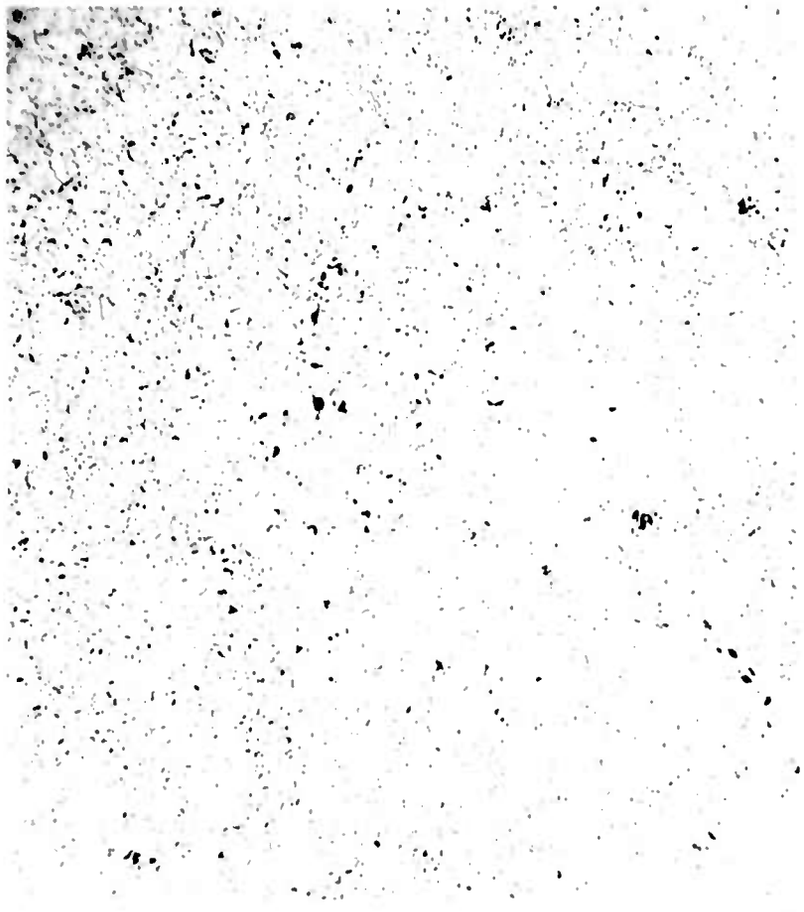

Figure 29 - Unfired Zirconium Carbide (Carborundum Co.)
Density 6.69 g/cc, etched X150

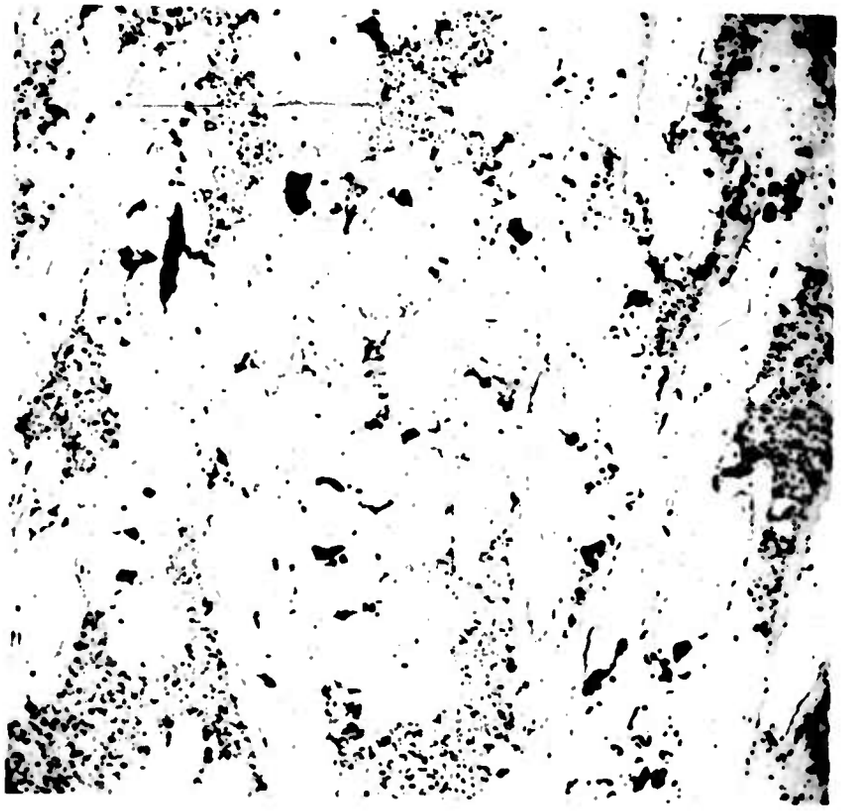

Figure 30 - Unfired Zirconium Carbide Reinforced with Tungsten Fibers, X150

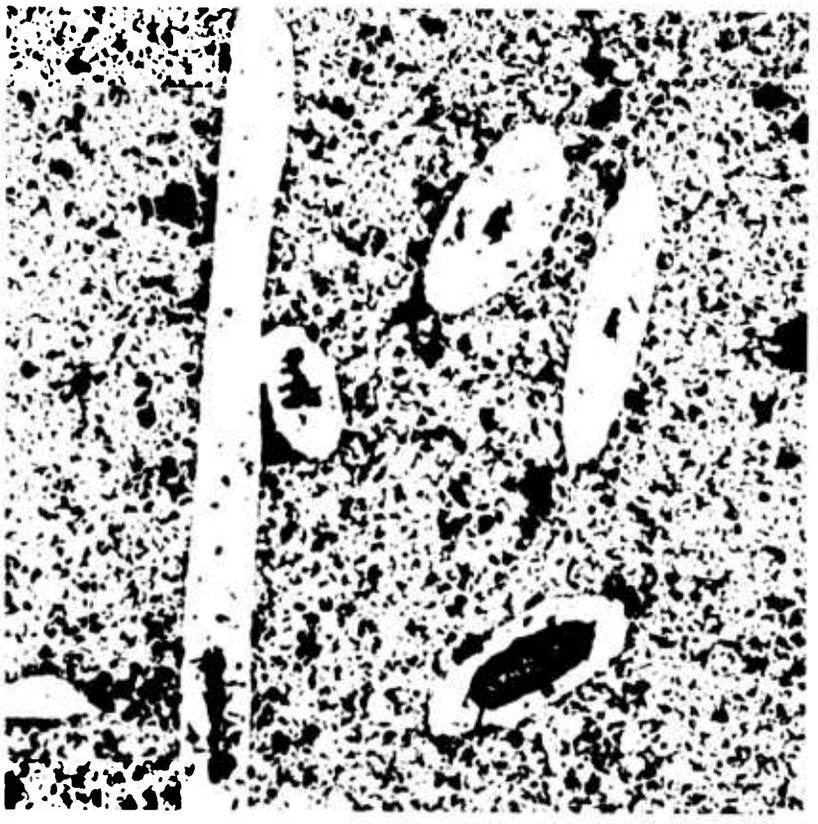

Figure 31 - Unfired Zirconium Carbide Reinforced with Tantalum Fibers, X150

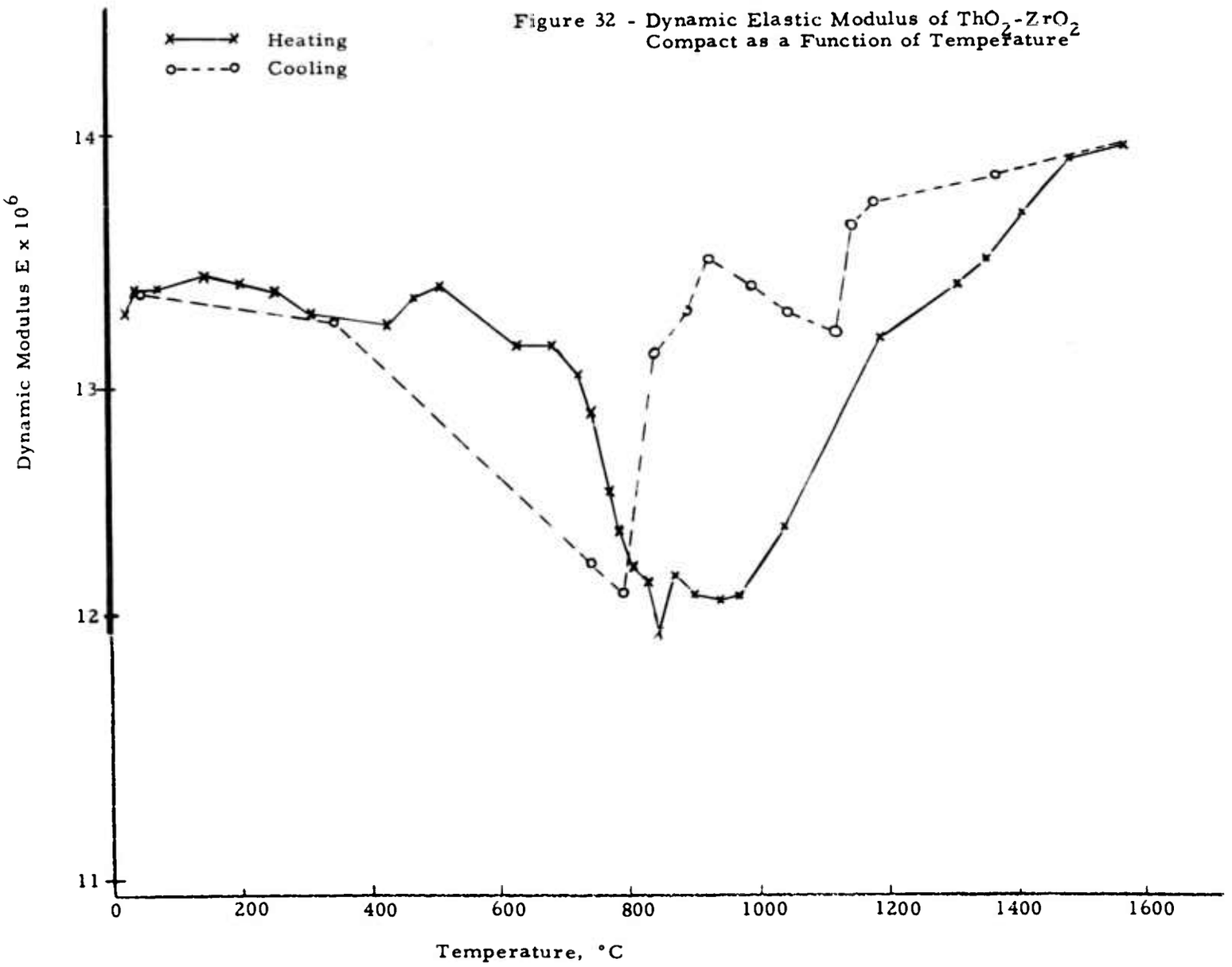

Figure 32 - Dynamic Elastic Modulus of ThO_2-ZrO_2 Compact as a Function of Temperature

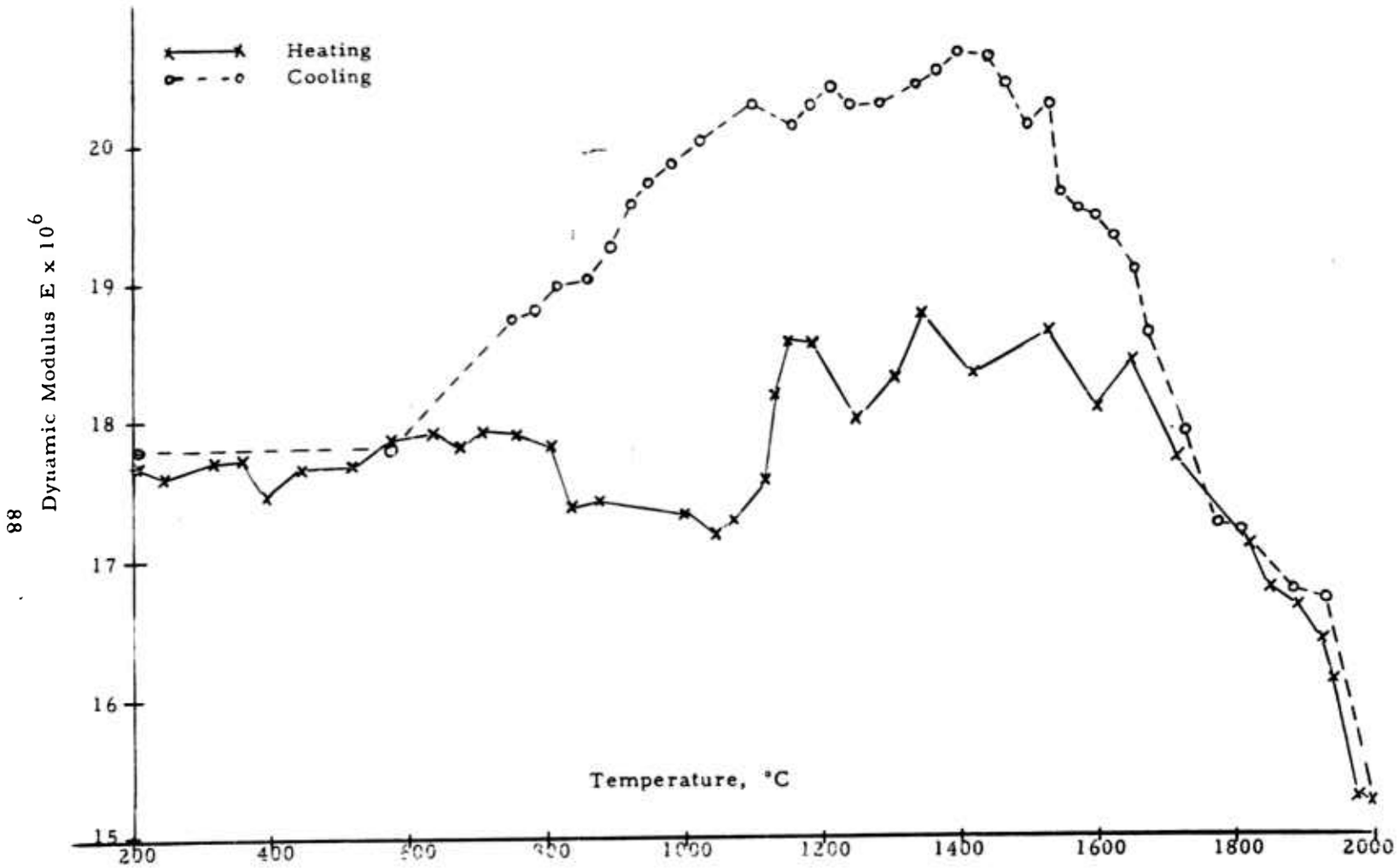

Figure 33 - Dynamic Elastic Modulus of Compact of ThO_2-ZrO_2 Reinforced with Tungsten Fibers as a Function of Temperature

Figure 34 - Hot Pressed Graphite, Test Sample AA-1, X150

Figure 35 - Untreated TSX, Test Sample BB-2, X150

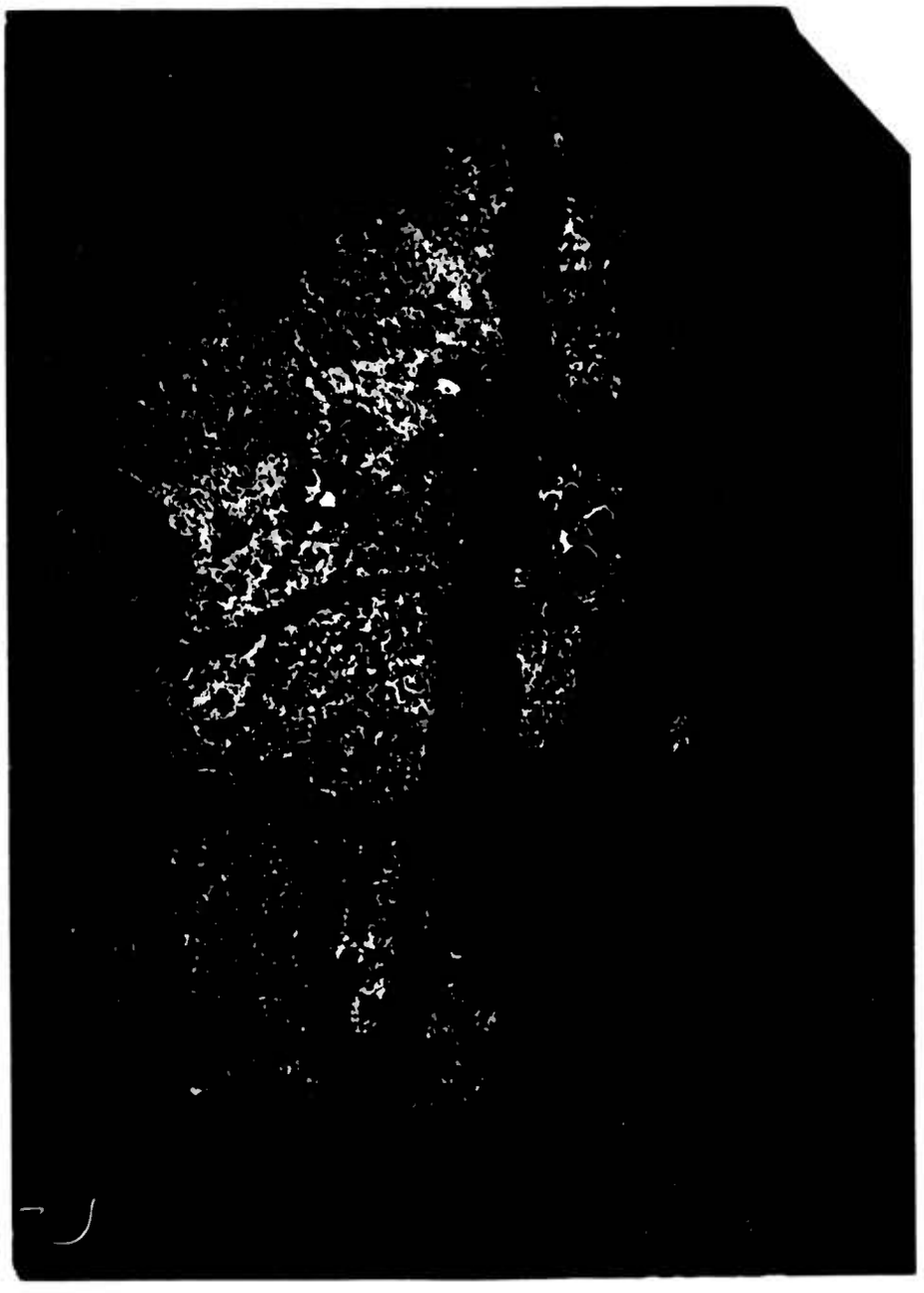

Figure 36 - Zirconium Carbide with Tantalum Fibers,
Test Sample DD-1, X50

Figure 37 - Thorium Oxide with Tungsten Fibers
Test Sample EE-2, X50

Figure 38 - Hot Pressed Graphite, Test Sample FF-2, X150

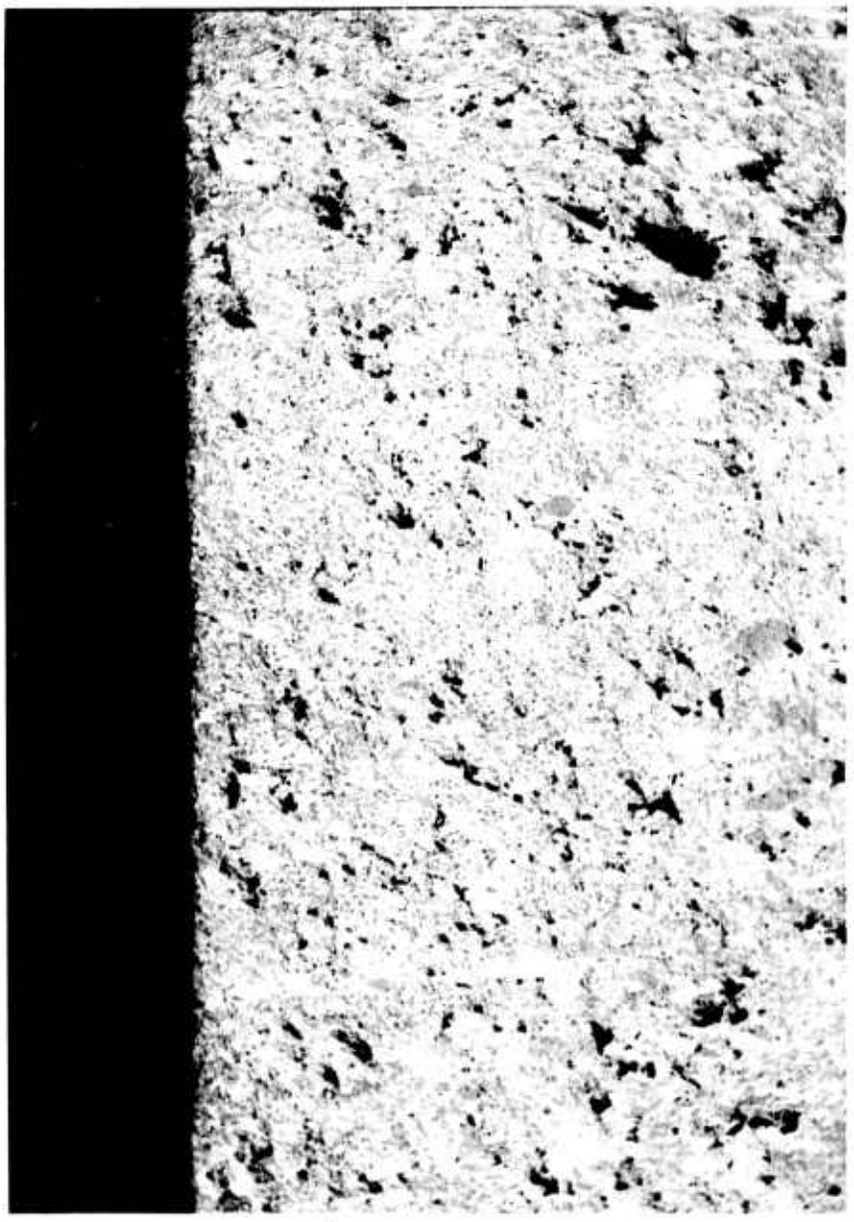

Figure 39 - ZT-4001, Test Nozzle GG-2, X150

Figure 40 - TSX Impregnated with Modified Furfuryl Compound, Test Sample HH-1, X150

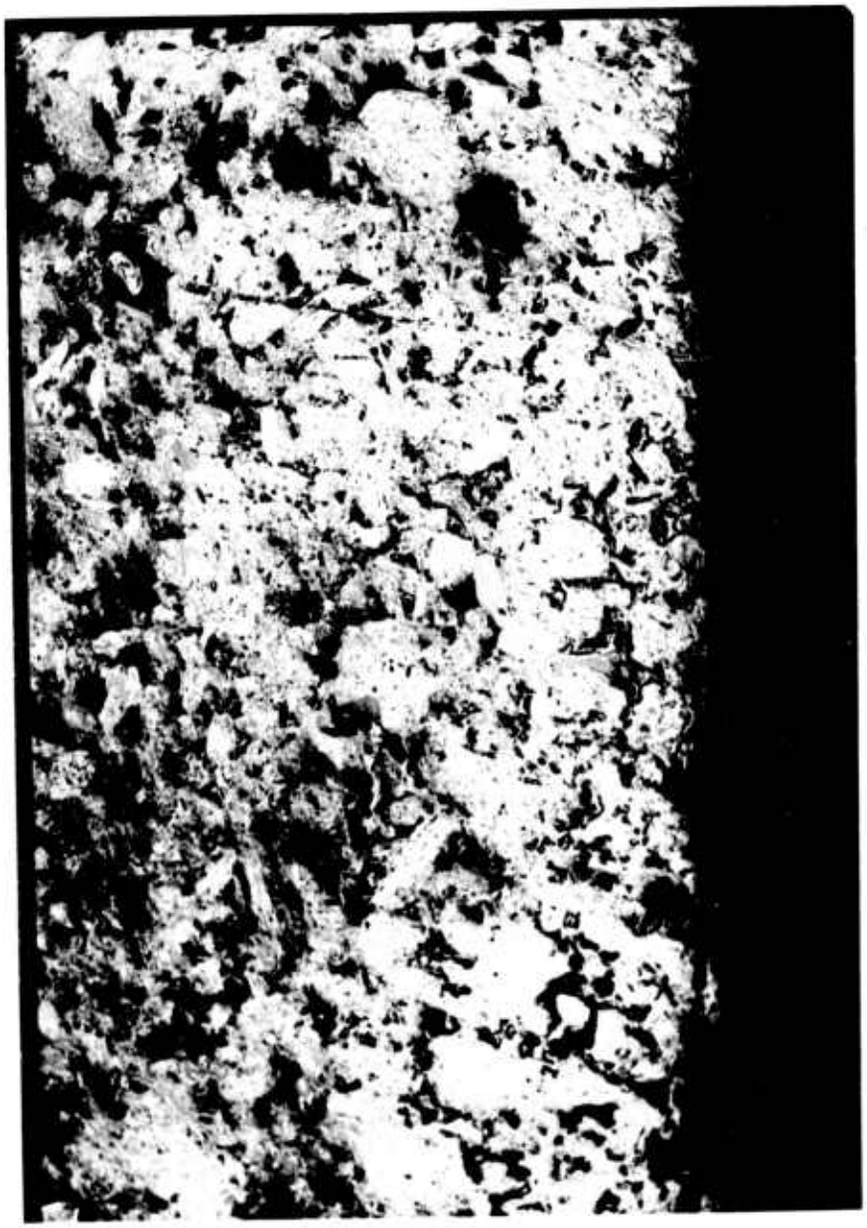

Figure 41 - ATJ Impregnated with Modified Furfuryl Compound, Test Sample II-2, X150

Figure 42 - Zirconium Carbide with Tungsten Fibers Coated with Tungsten, Test Sample KK-2, X50

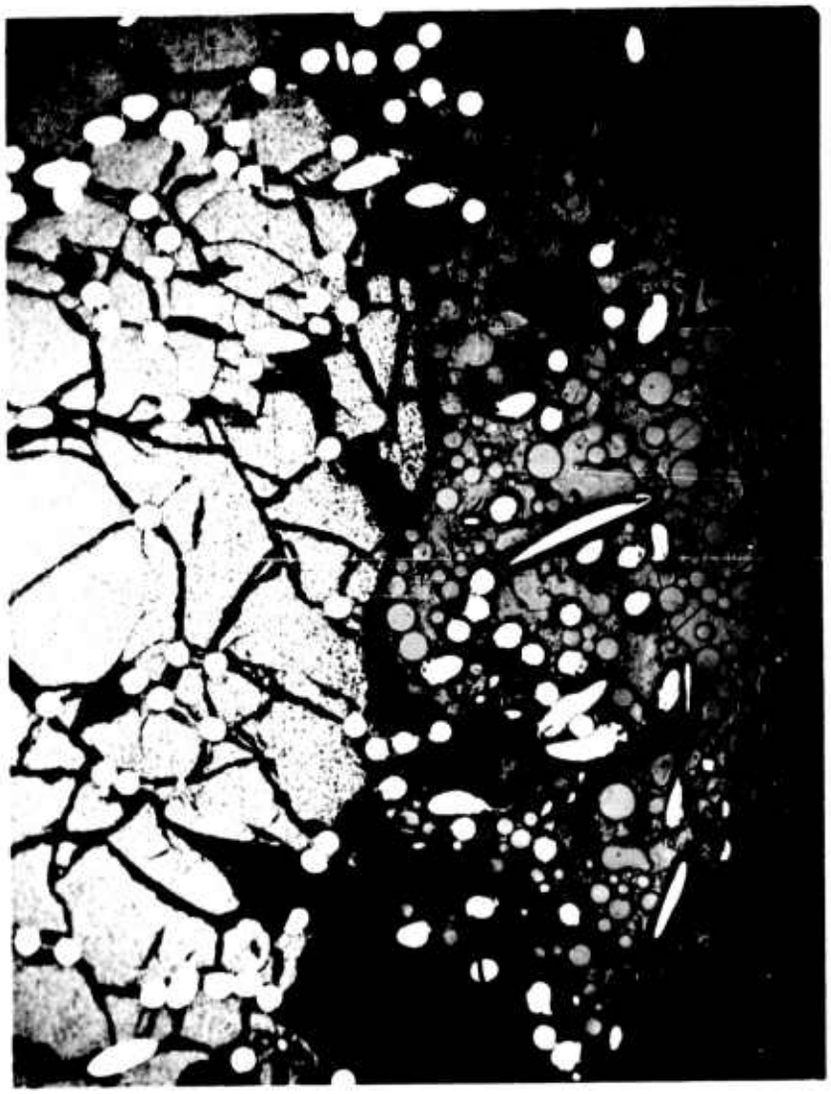

Figure 43 - Thorium Oxide with Tungsten Fibers Coated with Tungsten, Test Sample LL-2, X50

APPENDIX

THERMODYNAMIC ANALYSIS AND BALLISTIC PROPERTIES OF OXY-ACETYLENE EXPERIMENTAL TORCH

Initial conditions where O_2 and C_2H_2 are mixed, but not burned: (There is no significant thermodynamic difference between the two gas mixtures considered).

P = 27 psia

T = 530°R

A_{cr} = 0.0048 in^2

= 0.137 lb/st^3

$\dot{w}$ = 0.0024 lb/sec

r = 53.5 (ft-lb)/lb-°R

c_p = 0.281 btu/lb-°R

c_v = 0.212 btu/lb-°R

= 1.325

v = 520 fps

Final condition at the downstream end of sample:

P = 15 psia - assumed

T = 6000°R - estimated

A_{cr} = 0.049 in^2

T = 5470°R

v = 600 fps - calculated from energy equation

Calculated ballistic properties:

$T = \frac{\dot{w}}{g} v$ thrust, lbs.

$I_{sp} = v/g$ specific impulse, sec

$C_D = \frac{2}{+1}^{\frac{+1}{2(\ -1)}} \frac{g}{rT_c}$ discharge coefficient, sec^{-1}

$\dot{w} = C_D A_{cr} P_c$

$P_c = \frac{\dot{w}}{C_D A_{cr}}$ comparable rocket chamber pressure, psia

T = 0.04 lbs

I_{sp} = 20 lb-sec/lb

C_d = 6.4 (10^{-3}) sec^{-1}

P_c = 8 psia

$\dot{w}$ = 0.0024 lb/sec

T_c = 6500°R

REFERENCES

1 Y. Baskin and T. A. Greening, "Study of the Mechanism of Failure of Rocket Materials," WADC TR 58-152, Part I, (August 1958).

2 Y. Baskin and T. A. Greening, "Study of the Mechanism of Failure of Rocket Materials," WADC TR 58-152, Part I, Supplement I (January 1959).

3 Y. Baskin, R. F. Havell, and D. C. Schell, "Study of the Mechanism of Failure of Rocket Materials," WADC TR 58-152, Part II (in press).

4 "Oxy-Acetylene Welding and Cutting Instruction Course," Air Reduction Company (1951).

5 L. E. J. Robert, E. A. Harper, and C. T. Small, AERE c/r 882, Harwell (1958).

6 G. E. Bacon, Jour. Appl. Chem., Vol. 6, p 660 (1956).

7 S. W. Bradstreet, "Graphite Technology," WADC TR 58-503 (January 1959).

8 S. A. Bortz and H. H. Lund, "Evaluation of a Tension Test for Brittle Materials," Proc. Fourth Conference on Carbon (1960).

9 G. R. Hennig and M. A. Kantner, "Effect of Lattice Defects on Reactivity of Graphite," Fourth International Symposium on Reactivity of Solids (June 1960).

10 Y. Baskin, C. A. Arenberg, and J. H. Handwerk, "Thoria Reinforced by Metal Fibers," Am. Ceram. Soc. Bull., Vol. 38, p 345 (1959).

11 J. F. Lynch, D. J. Bowers, and W. H. Duckworth, "Characterization of Nozzle Failure Mechanisms," WADD TR 60-532 (April 1960).

12 J. F. Lynch, D. J. Bowers, and W. H. Duckworth, "Characterization of Nozzle Failure Mechanisms," Sixth Quarterly Report (September 1960).

13 "Research and Development on Advanced Graphite Materials," WADD Technical Note 61-18 (April 1961).

Aeronautical Systems Division, Dir/Materials and Processes, Metals and Ceramics Lab, Wright-Patterson AFB, Ohio.
Rpt Nr ASD-TDR-62-314. STUDY OF THE MECHANISM OF FAILURE OF ROCKET MATERIALS AND MATERIALS RESEARCH. Final report, May 62, 108p. incl illus., tables, 13 refs.

Unclassified Report

Rocket failure mechanisms in conjunction with the development of nozzle materials for solid propellant motors is discussed. Testing graphite in an oxy-acetylene torch and the effects of purity, density, orientation, and microstructure on erosion-resistance were evaluated. Erosion decreased with greater purity. New graphite materials were developed and evaluated including hot pressed compositions and impregnated bodies.

Suitability of ZrC as a nozzle material was evaluated. Incorporation of Ta and W fibers in ZrC results in considerable improvement in resistance to thermal spalling although not sufficient to prevent cracking. Thoria-base bodies reinforced with W fibers were studied.

Ten promising materials were fabricated into rocket nozzles and tested in static motor stands. Erosion performance is presented along with analysis of failure mechanisms.

(over)

1. Nozzle materials
2. Graphite
3. Refractory metals
I. AFSC Project 7350, Task 735001
II. Contract AF 33(616)-7048
III. Armour Research Foundation of Ill. Inst. of Technology, Chicago, Ill.
IV. Y. Baskin, D. C. Schell, W. K. Sumida
V. Aval fr OTS
VI. In ASTIA collection

Aeronautical Systems Division, Dir/Materials and Processes, Metals and Ceramics Lab, Wright-Patterson AFB, Ohio.
Rpt Nr ASD-TDR-62-314. STUDY OF THE MECHANISM OF FAILURE OF ROCKET MATERIALS AND MATERIALS RESEARCH. Final report, May 62, 108p. incl illus., tables, 13 refs.

Unclassified Report

Rocket failure mechanisms in conjunction with the development of nozzle materials for solid propellant motors is discussed. Testing graphite in an oxy-acetylene torch and the effects of purity, density, orientation, and microstructure on erosion-resistance were evaluated. Erosion decreased with greater purity. New graphite materials were developed and evaluated including hot pressed compositions and impregnated bodies.

Suitability of ZrC as a nozzle material was evaluated. Incorporation of Ta and W fibers in ZrC results in considerable improvement in resistance to thermal spalling although not sufficient to prevent cracking. Thoria-base bodies reinforced with W fibers were studied.

Ten promising materials were fabricated into rocket nozzles and tested in static motor stands. Erosion performance is presented along with analysis of failure mechanisms.

(over)

1. Nozzle materials
2. Graphite
3. Refractory metals
I. AFSC Project 7350, Task 735001
II. Contract AF 33(616)-7048
III. Armour Research Foundation of Ill. Inst. of Technology, Chicago, Ill.
IV. Y. Baskin, D. C. Schell, W. K. Sumida
V. Aval fr OTS
VI. In ASTIA collection

Aeronautical Systems Division, Dir/Materials and Processes, Metals and Ceramics Lab. Wright-Patterson AFB, Ohio.
Rpt Nr ASD-TDR-62-314. STUDY OF THE MECHANISM OF FAILURE OF ROCKET MATERIALS AND MATERIALS RESEARCH. Final report, May 62. 106p. incl illus., tables, 13 refs.

Unclassified Report

Rocket failure mechanisms in conjunction with the development of nozzle materials for solid propellant motors is discussed. Testing graphite in an oxy-acetylene torch and the effects of purity, density, orientation, and microstructure on erosion-resistance were evaluated. Erosion decreased with greater

(over)

1. Nozzle materials
2. Graphite
3. Refractory metals
I. AFSC Project 7350, Task 735001
II. Contract AF 33(616)-7048
III. Armour Research Foundation of Ill. Inst. of Technology, Chicago, Ill.
IV. Y. Baskin, D. C. Schell, K. K. Sumida
V. Aval fr OTS
VI. In ASTIA collection

Aeronautical Systems Division, Dir/Materials and Processes, Metals and Ceramics Lab. Wright-Patterson AFB, Ohio.
Rpt Nr ASD-TDR-62-314. STUDY OF THE MECHANISM OF FAILURE OF ROCKET MATERIALS AND MATERIALS RESEARCH. Final report, May 62. 106p. incl illus., tables, 13 refs.

Unclassified Report

Rocket failure mechanisms in conjunction with the development of nozzle materials for solid propellant motors is discussed. Testing graphite in an oxy-acetylene torch and the effects of purity, density, orientation, and microstructure on erosion-resistance were evaluated. Erosion decreased with greater

(over)

purity. New graphite materials were developed and evaluated including hot pressed compositions and impregnated bodies.

Suitability of ZrC as a nozzle material was evaluated. Incorporation of Ta and W fibers in ZrC results in considerable improvement in resistance to thermal spalling although not sufficient to prevent cracking. Thoria-base bodies reinforced with W fibers were studied.

Ten promising materials were fabricated into rocket nozzles and tested in static motor stands. Erosion performance is presented along with analysis of failure mechanisms.

1. Nozzle materials
2. Graphite
3. Refractory metals
I. AFSC Project 7350, Task 735001
II. Contract AF 33(616)-7048
III. Armour Research Foundation of Ill. Inst. of Technology, Chicago, Ill.
IV. Y. Baskin, D. C. Schell, K. K. Sumida
V. Aval fr OTS
VI. In ASTIA collection